Article

Cell Host & Microbe

# The Glycolytic Pyruvate Kinase Is Recruited Directly into the Viral Replicase Complex to Generate ATP for RNA Synthesis

## Graphical Abstract

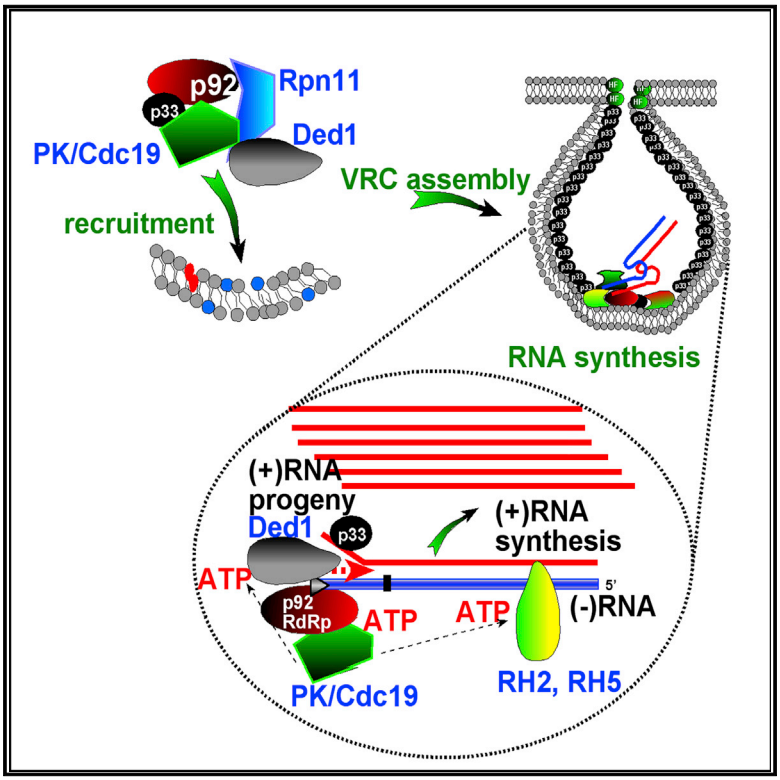


## Highlights

- The plant virus TBSV recruits the glycolytic pyruvate kinase (PK) to its replicase complex
- PK generates high levels of ATP within the viral replication compartment (VRC)
- ATP fuels the activity of co-opted cellular DEAD-box helicases within the VRC
- The high ATP concentration in the VRC facilitates rapid viral RNA synthesis

## Authors

Chingkai Chuang,
K. Reddisiva Prasanth, Peter D. Nagy

## Correspondence

pdnagy2@uky.edu

## In Brief

RNA viruses co-opt several host proteins to aid their replication in infected cells. Chuang et al. demonstrate that a small plant virus recruits the cellular glycolytic pyruvate kinase (PK) directly into the viral replicase complex. PK supplies ATP to fuel co-opted cellular helicases, which drives rapid viral RNA synthesis.

Chuang et al., 2017, Cell Host & Microbe *22*, 1–14
November 8, 2017 
https://doi.org/10.1016/j.chom.2017.10.004

CellPress

Please cite this article in press as: Chuang et al., The Glycolytic Pyruvate Kinase Is Recruited Directly into the Viral Replicase Complex to Generate ATP for RNA Synthesis, Cell Host & Microbe (2017), https://doi.org/10.1016/j.chom.2017.10.004

Cell Host & Microbe
Article



# The Glycolytic Pyruvate Kinase Is Recruited Directly into the Viral Replicase Complex to Generate ATP for RNA Synthesis

Chingkai Chuang,[1] K. Reddisiva Prasanth,[1] and Peter D. Nagy[1,2,*]
[1]Department of Plant Pathology, University of Kentucky, Plant Science Building, Lexington, KY 40546, USA
[2]Lead Contact
*Correspondence: pdnagy2@uky.edu
https://doi.org/10.1016/j.chom.2017.10.004

## SUMMARY

**Viruses accomplish their replication by exploiting many cellular resources, including metabolites and energy. Similarly to other (+)RNA viruses, tomato bushy stunt virus (TBSV) induces major changes in infected cells. However, the source of energy required to fuel TBSV replication is unknown. We find that TBSV co-opts the cellular glycolytic ATP-generating pyruvate kinase (PK) directly into the viral replicase complex to boost progeny RNA synthesis. The co-opted PK generates high levels of ATP within the viral replication compartment at the expense of a reduction in cytosolic ATP pools. The ATP generated by the co-opted PK is used to promote the helicase activity of recruited cellular DEAD-box helicases, which are involved in the production of excess viral (+)RNA progeny. Altogether, recruitment of PK and local production of ATP within the replication compartment allow the virus replication machinery an access to plentiful ATP, facilitating robust virus replication.**

## INTRODUCTION

RNA virus replication depends on the formation of large intracellular replication organelles, which requires major membrane remodeling and proliferation, retargeting of trafficking vesicles, and recruitment of numerous host proteins into the viral replicase complex (den Boon and Ahlquist, 2010; Fernández de Castro et al., 2016; Nagy and Pogany, 2011; Paul and Bartenschlager, 2015; Wang, 2015). Moreover, RNA viruses exploit host cells by utilizing cellular metabolites and energy needed for the production of a large number of viral progeny. Tomato bushy stunt virus (TBSV), similar to other (+)RNA viruses, induces major metabolic and structural changes in the infected cells; these changes include the aggregation of peroxisomal and ER membranes and the creation of membrane deformations through formation of hundreds of 40–70 nm spherules (vesicle-like structures in the boundary membrane of peroxisomes) that harbor the viral replicase (Barajas et al., 2014a; Fernández de Castro et al., 2017; Rochon et al., 2014). In addition, TBSV stabilizes the actin network by blocking the function of Cof1/Adf actin depolymerization factor and hijacks the Rab5-positive early endosomal vesicles (Nawaz-ul-Rehman et al., 2016; Xu and Nagy, 2016). Moreover, a large number of host proteins are co-opted to support various viral functions. These proteins include the endosomal sorting complex required for transport (ESCRT) machinery, heat shock protein 70 (Hsp70), glyceraldehyde-3-phosphate dehydrogenase (GAPDH), eukaryotic elongation factor 1A (eEF1A), eEF1Bγ, the DDX3-like Ded1, eIF4AIII-like RH2, and DDX5-like RH5 DEAD-box RNA helicases (Barajas et al., 2009a; Huang and Nagy, 2011; Li et al., 2010; Nagy, 2008; Sasvari et al., 2011; Serva and Nagy, 2006; Wang and Nagy, 2008). TBSV taps into lipid resources as well by inducing enrichment of sterols at the viral replication sites via stabilizing membrane contact sites. It also retargets phosphatidylethanolamine to the replication sites (Barajas et al., 2014b; Xu and Nagy, 2016). All these TBSV-induced robust changes in the cell require energy, likely in the form of ATP, the major energy source in the cell. However, the way TBSV obtains the energy to fuel these energy-consuming processes is currently not known.

Glycolysis is a major cytosolic metabolic pathway producing ATP and pyruvate from glucose (Vander Heiden et al., 2010). The last step of glycolysis is the production of pyruvate and ATP from PEP by pyruvate kinase. Glycolysis also contributes metabolites for various biosynthetic pathways, including lipid, amino acid, and nucleic acid production. Cancerous cells promote high-level glycolysis to support high rates of macromolecular synthesis (Stine and Dang, 2013; Vander Heiden et al., 2010). The glycolytic machinery is also critical for immune cell activation (Peng et al., 2016). Several viruses can enhance glucose uptake and upregulate the aerobic glycolytic pathway, which provides fast supply of ATP and metabolites to various viral processes (Diamond et al., 2010; Findlay and Ulaeto, 2015; Fontaine et al., 2015; Su et al., 2014; Teng et al., 2015).

Previous genome-wide screens in a yeast model host have identified several components of the glycolytic pathway that affected TBSV replication (Jiang et al., 2006; Panavas et al., 2005b; Nawaz-ul-Rehman et al., 2013). One of these enzymes, GAPDH, has been shown to be recruited to the site of replication; GAPDH facilitates viral RNA synthesis via its RNA binding function (Huang and Nagy, 2011; Wang and Nagy, 2008). Proteomic screens also identified pyruvate kinase (PK, Cdc19p in yeast), which was pulled down with the tombusviral p92 RdRp (Pogany and Nagy, 2012).

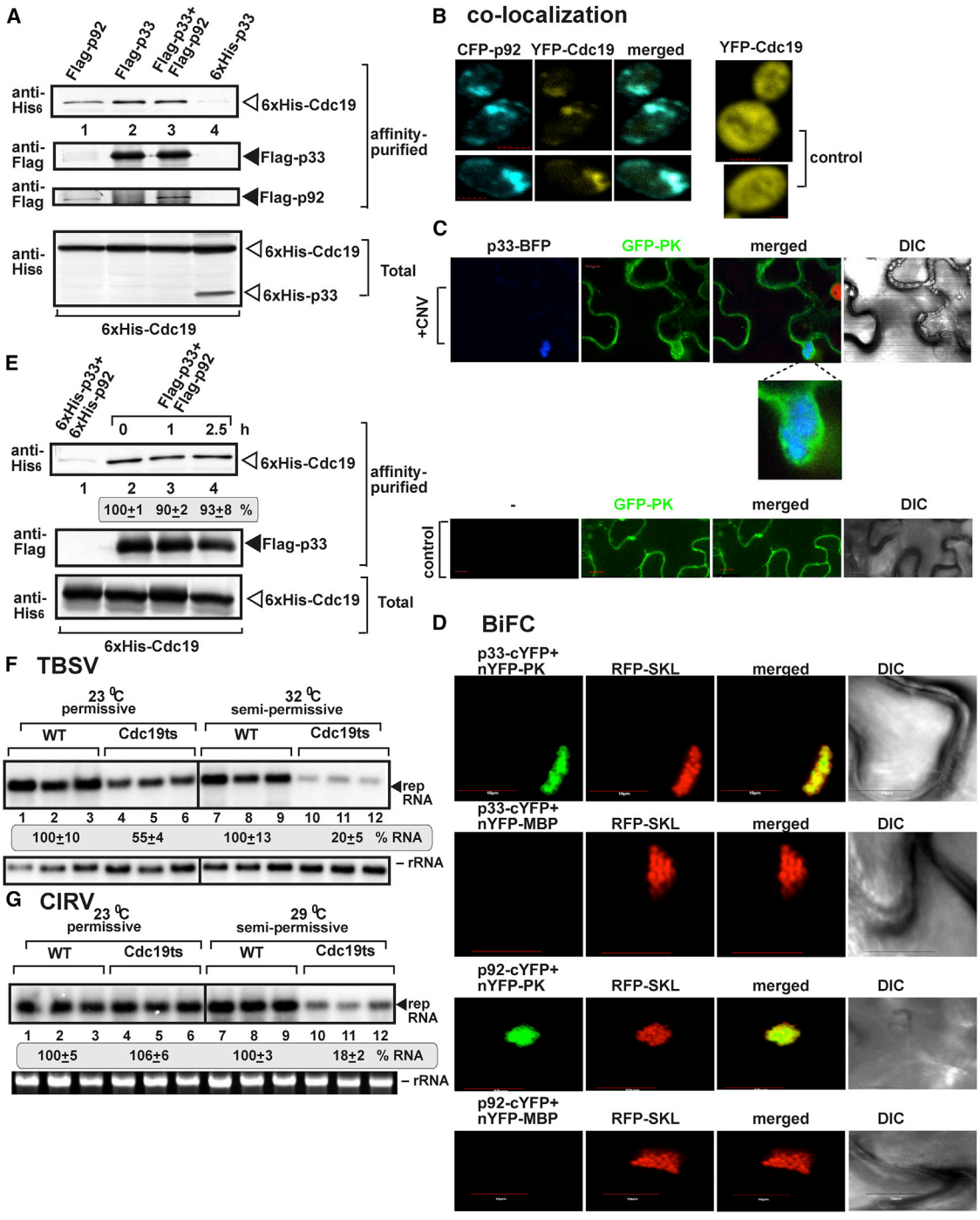


**Figure 1. Recruitment of the Cytosolic Pyruvate Kinase into the Viral Replicase via Interaction with p33 and p92$^{pol}$ Replication Proteins in Yeast and Plant Cells**

(A) Co-purification of the yeast Cdc19p with the viral replicase complex. Top: western blot analysis of co-purified, $His_6$-tagged Cdc19p with FLAG-affinity purified p33 and FLAG-p92$^{pol}$ from membrane fraction of WT yeast. Cdc19p was detected with anti-His antibody. The negative control was $His_6$ tagged and p33 purified from yeast extracts using a FLAG-affinity column (lane 4). Middle two: western blots of purified FLAG-p33 and FLAG-p92$^{pol}$ detected with anti-FLAG antibody. Bottom: western blot of $His_6$-Cdc19p and $His_6$-p33 (lane 4) proteins in the total yeast extracts using anti-His antibody. Note that the background signal in lanes 2 and 3 in the third panel comes from the SDS-resistant oligomeric forms of FLAG-p33.

(B) The partial co-localization of TBSV CFP-tagged p92$^{pol}$ with the YFP-tagged Cdc19p in WT yeast cells is detected by confocal laser microscopy. The images on the right show the cytosolic distribution of YFP-Cdc19p in the absence of viral components in WT yeast cells.

(C) Confocal laser microscopy was used to detect partial co-localization of TBSV BFP-tagged p33 replication protein with the GFP-NbPK protein in *N. benthamiana* cells. The plants were inoculated with the closely related CNV to induce large replication compartments (+CNV image). The red dot represents the

*(legend continued on next page)*

The above findings suggest that cytosolic tombusviruses might be able to reprogram the glycolytic pathway to fuel various viral processes during infection. In the current work, we discovered that TBSV recruits the glycolytic pyruvate kinase into the viral replicase to boost viral RNA replication. The subversion of PK occurs through direct interaction with the viral replication proteins, although an additional host protein is also involved in this process. We provide evidence that the ATP generated by the co-opted PK is used to promote the helicase activity of recruited cellular helicases, which are involved in viral (+)-strand synthesis. Thus, glycolysis and the generated ATP are directly and locally exploited by tombusviruses within the viral replication compartment to support virus replication in infected cells.

## RESULTS

### Tombusvirus Replication Proteins Interact with the Glycolytic Pyruvate Kinase in Yeast and Plant Cells

Previous genome-wide and proteomic screens have identified several glycolytic enzymes that affected TBSV replication in a yeast model host and interacted with the viral replication proteins (Jiang et al., 2006; Panavas et al., 2005b; Pogany and Nagy, 2012; Nawaz-ul-Rehman et al., 2013). To test if the ATP-generating pyruvate kinase (PK/Cdc19p) interacts directly with the viral replication proteins, we first performed co-purification experiments with affinity-tagged viral replication proteins from yeast membranes. Western blot analysis of the purified functional replicase complex revealed the presence of Cdc19p (Figure 1A, lane 3). We also found that Cdc19p was co-purified with either TBSV p92 RdRp or p33 RNA chaperone proteins, suggesting direct interaction of Cdc19p with the viral replication proteins (Figure 1A). In contrast, Cdc19p was not co-purified with Flag-GFP control (Figure S1A). Second, pulldown experiments defined that the C-terminal protein interaction domain of the p33 replication protein, which is involved in interaction with other p33 and p92 molecules (Rajendran and Nagy, 2006), binds to Cdc19p *in vitro* (Figures S1B and S1C). On the other hand, Cdc19p might bind to p33 via more than one domain, because each of the deletion constructs showed lesser interactions with p33 than the full-length Cdc19p (Figure S1D), which can form a tetramer (Valentini et al., 2000). Third, we conducted confocal microscopy experiments with fluorescently tagged replication protein and PK/Cdc19p in yeast and plant cells; this revealed efficient re-localization of PK/Cdc19p to the replication compartment visualized as large punctate structures containing $p92^{pol}$ and p33 (Figures 1B and 1C). Fourth, to confirm that the subcellular site of interaction between PK/Cdc19p and the replication proteins is indeed the replication compartment, we used BiFC. This revealed that the location of the replication protein-PK/Cdc19p interaction is the TBSV-induced aggregated peroxisomes visualized by the RFP-SKL marker in plant cells (Figure 1D). Therefore, we propose that TBSV co-opts PK/Cdc19p into the viral replication compartment through direct interaction with the viral replication proteins in yeast and plant cells.

Next, we tested whether PK/Cdc19p is a permanent component of the viral replicase complex through inhibition of new VRC formation (via blockage of yeast translation through cycloheximide), followed by purification of the viral replicase from yeast cells at various time points. Interestingly, the co-purified Cdc19p level did not change in comparison with FLAG-p33 throughout 2.5 hr (Figure 1E), suggesting that Cdc19p is a permanent member of the membrane-bound viral replicase.

### Pyruvate Kinase Is Required for Tombusvirus Replication in Yeast and Plant Cells

Partial inactivation of a temperature-sensitive (ts) mutant of *CDC19* in haploid yeast revealed ~5-fold inhibition of TBSV replicon RNA (repRNA) accumulation (Figure 1F, lanes 10–12), confirming that PK is critical for TBSV replication in yeast. The related carnation Italian ringspot virus (CIRV), which replicates on the boundary membranes of mitochondria, was also inhibited in $cdc19^{ts}$ yeast (Figure 1G, lanes 10–12), suggesting that PK/Cdc19 is required for tombusvirus replication in different subcellular environments. Interestingly, we found that the newly made (+)repRNA levels decreased by ~5-fold, while the (−)repRNA, which is part of the dsRNA replication intermediate (Kovalev et al., 2014), did not change in $cdc19^{ts}$ yeast grown at semi-permissive temperature (Figure 2A, lanes 10–12). Complementation via expression of the wild-type (WT) copy of *CDC19* from a plasmid in $cdc19^{ts}$ yeast confirmed that Cdc19p affects (+) RNA levels, while the (−)RNA level is not affected (Figure 2B, lanes 15 and 16 versus 13 and 14). Over-expression of Cdc19p in WT yeast increased TBSV (+)repRNA accumulation by ~50% (Figure 2B, lanes 3 and 4 and lanes 11 and 12), whereas (−)RNA accumulation did not change (Figure 2B, lanes 3, 4, 11, and 12), suggesting specific stimulatory role of PK/Cdc19

nucleus due to the expression of RFP-tagged fibrillarin. The control plants were not infected with CNV and lacked BFP-p33. Expression of the above proteins from the 35S promoter was achieved after co-agro-infiltration of *N. benthamiana* leaves. Scale bars represent 5 μm.

(D) Top image: *In planta* interaction between TBSV p33-cYFP replication protein and the nYFP-NbPK protein was detected by BiFC. Co-localization of RFP-SKL (peroxisomal luminar marker) with the BiFC signal (see merged image) demonstrates that the interaction between the p33 replication protein and NbPK occurs in the replication compartment. Expression of the above proteins from the 35S promoter was done after co-agro-infiltration into *N. benthamiana* leaves. Note that the plants were infected with TBSV to induce the replication compartment in cells. We also observed *in planta* interaction between TBSV p92-cYFP replication protein and the nYFP-NbPK protein by BiFC (third panel). Control BiFC experiments included nYFP-MBP protein in combination with p33-cYFP (second panel) or p92-cYFP (fourth panel). Scale bars represent 10 μm.

(E) PK/Cdc19p is a permanent component in the VRCs. The formation of new VRCs in WT yeast was blocked via inhibition of cellular translation by cycloheximide. Top: western blot analysis shows the co-purified $His_6$-Cdc19p with the viral replicase FLAG affinity purified from the membrane fraction at the shown time points. Middle: western blot analysis of the purified FLAG-p33 with anti-Flag antibody. Bottom: western blot analysis of $His_6$-Cdc19p in the total yeast lysates with anti-His antibody. See further details in (A). Each experiment was repeated three times.

(F and G) Reduced TBSV (F) and CIRV (G) repRNA accumulation in $cdc19^{ts}$ yeast. Top images: Northern blot analyses show TBSV and CIRV repRNA accumulation in WT and $cdc19^{ts}$ yeast grown at permissive and semi-permissive temperatures. The accumulation level of repRNA was normalized based on 18S rRNA levels (bottom). Each experiment was performed three times.

All + and − values denote standard deviation.

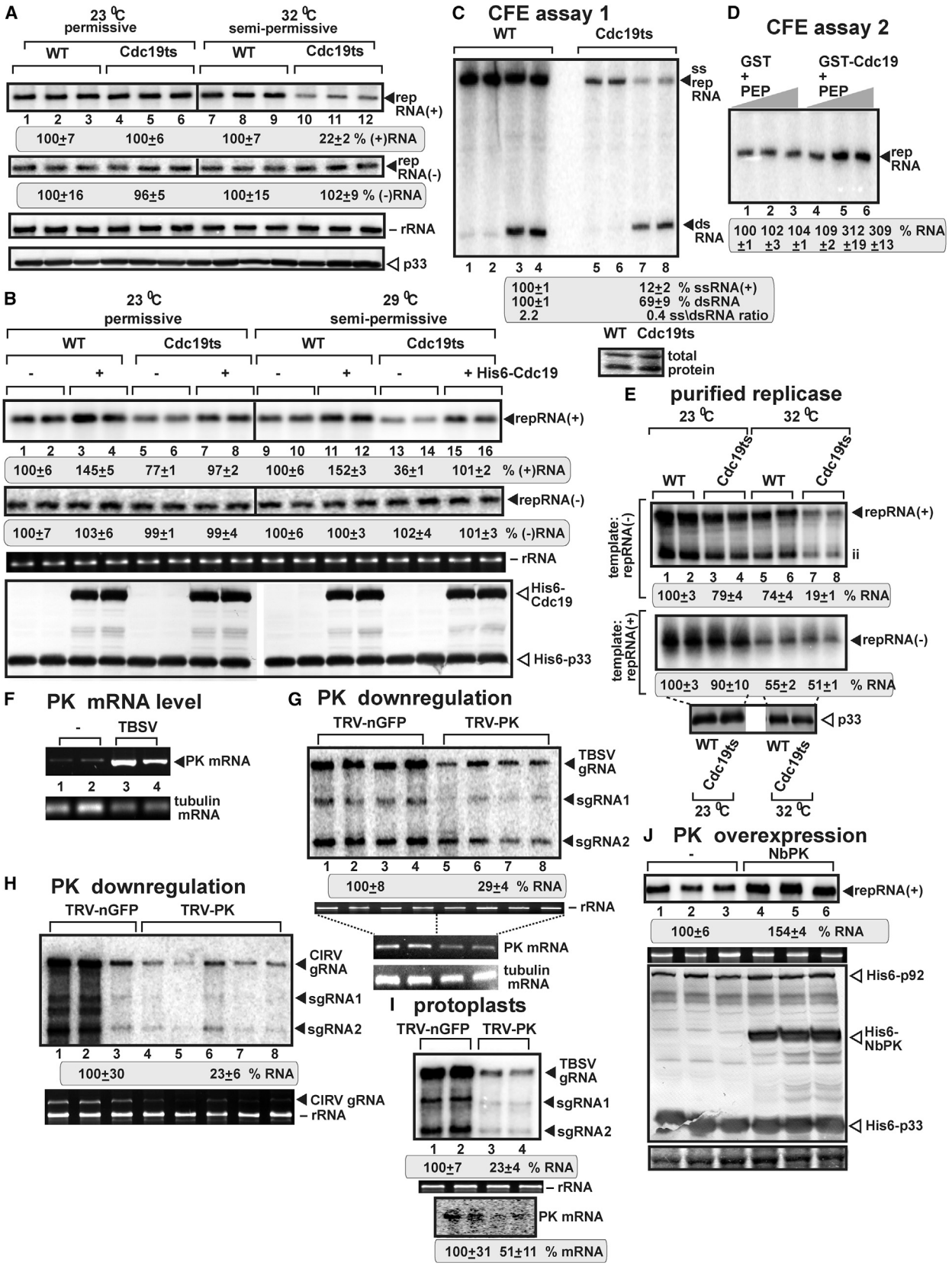


*(legend on next page)*

in viral (+)RNA synthesis. When yeasts were grown on glycerol, a non-fermentable carbon source, then the *cdc19*$^{ts}$ strain supported TBSV repRNA replication at the semi-permissive temperature to a comparable level with WT yeast (Figure S2), suggesting that the co-opted PK/Cdc19 provides pro-viral function only during active glycolysis.

To further demonstrate that PK is required for viral RNA replication, we obtained cell-free extracts (CFE) from WT and *cdc19*$^{ts}$ yeast to reconstitute the TBSV replicase *in vitro* based on purified recombinant TBSV proteins. The CFE-based assay, which supports a single full cycle of RNA replication (Pogany et al., 2008), showed an ~8-fold reduction in (+)RNA production with a 0.4 ratio of (+)RNA product to dsRNA replication intermediate obtained with CFE from *cdc19*$^{ts}$; this is in comparison with a 2.2 ratio obtained with the WT CFE (Figure 2C, lanes 7 and 8 versus 3 and 4). Therefore, the *in vitro* replication results support the important role of PK/Cdc19 in viral (+)RNA production. Also, addition of affinity-purified recombinant GST-Cdc19 to the WT CFE enhanced *in vitro* repRNA replication by ~3-fold (Figure 2D, lanes 5 and 6). The purified replicase from *cdc19*$^{ts}$ yeast cultured at semi-permissive temperature showed a ~4-fold reduction in activity in comparison with the similar preparation obtained from WT yeast programmed with (−)RNA template (Figure 2E, top). The *in vitro* activity of these replicase preparations were comparable when programmed with the (+)RNA template (Figure 2E, middle). Overall, the various *in vivo* and *in vitro* results support a major pro-viral role for PK/Cdc19 in tombusvirus (+)RNA synthesis.

To explore if tombusviruses depend on co-opted PK in plants, we first analyzed PK mRNA levels in TBSV-infected versus mock-treated *Nicotiana benthamiana* leaves. RT-PCR results showed upregulation of PK mRNA level in TBSV-infected leaves (Figure 2F), suggesting that TBSV replication induces increased PK expression. Gene-silencing-based downregulation of PK level in *N. benthamiana* plants led to 71% and 77% reduction of TBSV genomic (g)RNA and CIRV gRNA, respectively (Figures 2G and 2H, lanes 5–8). A TBSV replication assay based on protoplasts (single, cell-wall-free plant cells) also showed a 77% decrease in gRNA level when protoplasts were obtained from NbPK-silenced *N. benthamiana* plants (Figure 2I). In contrast, over-expression of the *N. benthamiana* PK enhanced TBSV repRNA accumulation by 54% in yeast (Figure 2J, lanes 4–6), confirming the pro-viral function of PK in tombusvirus replication.

## Robust Generation of ATP by the Co-opted Pyruvate Kinase in the Tombusvirus Replication Compartment

The co-opted PK/Cdc19 likely generates ATP within the viral replication compartment to fuel viral RNA synthesis. To estimate the ATP level within the replication compartment, we tagged p92$^{pol}$ replication protein with ATeam, a FRET-based ATP biosensor, which can indicate local ATP levels in various subcellular compartments (Imamura et al., 2009). Intracellular

**Figure 2. The Role of the Co-opted Cytosolic PK/Cdc19 in Tombusvirus Replication**

(A) Top image: northern blot analysis shows decreased TBSV (+)repRNA accumulation in a yeast strain (*cdc19*$^{ts}$) grown at semi-permissive temperature. Middle image: northern blot analysis reveals comparable TBSV (−)repRNA accumulation in a yeast strain (*cdc19*$^{ts}$) grown at semi-permissive temperature versus the WT strain. The accumulation level of repRNA was normalized based on 18S rRNA levels (third panel). The accumulation of His$_6$-p33 is measured by western blotting and anti-His$_6$ antibody.

(B) Complementation assay with plasmid-borne expression of His$_6$-Cdc19 in *cdc19*$^{ts}$ yeast grown at either permissive or semi-permissive temperatures. His$_6$-Cdc19 was expressed from the *GAL1* promoter. Top: northern blot analysis of (+)repRNA and (−)repRNA levels; middle: ethidium-bromide stained gel with ribosomal RNA, as a loading control; bottom: western blot analysis using anti-His antibody. See further details in (A).

(C) Reduced (+)RNA production by the tombusvirus replicase assembled *in vitro* in CFEs prepared from *cdc19*$^{ts}$ yeast grown at semi-permissive temperature. Purified recombinant p33 and p92$^{pol}$ replication proteins of TBSV and *in vitro* transcribed TBSV DI-72 (+)repRNA were added to the CFEs prepared from the shown yeast strains. Non-denaturing PAGE analysis shows the $^{32}$P-labeled TBSV repRNA products, including the (+)repRNA progeny and the dsRNA replication intermediate, made by the reconstituted replicases. Lanes 1 and 2 and lanes 5 and 6 contain heat-denatured samples of aliquots used in lanes 3 and 4 and lanes 7 and 8, respectively, to confirm the dsRNA nature of the replication products. Bottom image: The CFEs contained the same amounts of total yeast proteins.

(D) The effect of the addition of purified recombinant GST-Cdc19 on the *in vitro* activity of the reconstituted replicase in WT CFE in the presence of PEP substrate and ADP.

(E) Reduced (+)RNA synthesis by the purified tombusvirus replicase from *cdc19*$^{ts}$ yeast grown at semi-permissive temperature. The membrane-bound replicase complex was collected by centrifugation, followed by solubilization and FLAG-affinity purification from yeasts. Representative denaturing gel of $^{32}$P-labeled RNA products synthesized by the purified tombusvirus replicase *in vitro.* Top image: The *in vitro* assays were programmed with RI/III (−)repRNA. Middle image: The *in vitro* assays were programmed with RIV (+)repRNA. Note that the original viral template RNA in the replicase from yeast is removed during replicase solubilization/purification. Bottom image: western blot analysis shows the comparable amounts of p33 replication proteins in each affinity-purified replicase sample.

(F) Upregulation of PK expression in TBSV-infected *N. benthamiana* leaves. The mRNA levels for the cytosolic PK were estimated by semi-quantitative RT-PCR in total RNA samples obtained from either TBSV or mock-infected *N. benthamiana* leaves. Tubulin mRNA was used as a control (second panel).

(G and H) VIGS-based knockdown of *PK* mRNA level inhibits the accumulation of tombusvirus RNA in *N. benthamiana*. Top panels: northern blot analysis of total RNA samples obtained from *N. benthamiana* leaves to show the accumulation of TBSV gRNA and sgRNAs in (G) and the mitochondria-replicating CIRV RNAs in (H). Middle images: ethidium-bromide stained gels show ribosomal RNA level. Bottom two images in (G) show the semi-quantitative RT-PCR analysis of the PK mRNA and tubulin mRNA (as a control) levels in the VIGS plants. We chose the 12th day after VIGS to inoculate the upper, systemically silenced leaves with TBSV virions or agro-infiltrate with pGD-CIRV. Samples for RNA extractions were taken 1 day (TBSV) and 2.5 days (CIRV) post-inoculation from the inoculated leaves. The control experiments included the TRV2-nGFP vector. Each experiment was performed three times.

(I) Inhibition of TBSV replication in protoplasts obtained from PK-silenced *N. benthamiana*. A VIGS approach with agrobacterium-mediated TRV2-PK expression was used to knockdown NbPK mRNA level (bottom image, northern blot) and on the 11th day, protoplasts were isolated from the upper leaves, followed by electroporation of TBSV RNA. Twenty-four hr later, total RNA was analyzed by northern blotting (top image).

(J) The effect of over-expression of *Nb* pyruvate kinase PK on TBSV repRNA accumulation in yeast. The plasmid-borne His$_6$-NbPK was expressed from *TEF1* promoter in BY4741 (WT) yeast. Top image: northern blot analysis of repRNA accumulation. Middle image: agarose gel stained with ethidium-bromide to visualize ribosomal RNA (rRNA) levels in each sample as a loading control. Bottom image: The accumulation levels of His$_6$-p33, His$_6$-p92 and His$_6$-NbPK were measured by western blotting and anti-His$_6$ antibody.

All + and − values denote standard deviation.

expression of ATeam-p92 can measure ATP levels via FRET due to the conformational change in the enhanced ε subunit of the bacterial $F_0F_1$-ATP synthase upon ATP binding without ATP hydrolysis. In the ATP-bound form the ε subunit draws the CFP and YFP fluorescent tags into proximity, increasing FRET, whereas in the ATP-free stage the extended conformation of the ε subunit places CFP and YFP at a distal position, leading to a low FRET signal in confocal laser microscopy (Figure 3A). In this ATP biosensor system, ATP concentration is linearly correlated with the YFP:CFP ratio within the detection limitation (Imamura et al., 2009). The ATeam-tagged p92 is a fully functional RdRp (Figure S3A) that localizes to the peroxisomal membrane (Figure S3B). The ATP level within the TBSV replication compartment was 4-fold higher in WT yeast than in *cdc19*$^{ts}$ yeast at the semi-permissive temperature (29 °C, Figure 3B). The difference in ATP accumulation within the replication compartment in WT yeast versus *cdc19*$^{ts}$ yeast was smaller at the permissive temperature (Figure 3C). Expression of the low-sensitive variant of ATeam (Imamura et al., 2009) as a p92 fusion protein (ATeam$^{RK}$-p92) showed low FRET values within the replication compartment in both WT and *cdc19*$^{ts}$ yeasts (Figures 3B and S3C), confirming that the FRET data is derived from the ATP biosensor in this assay. Interestingly, the mitochondria-replicating CIRV also accumulated a level of ATP that was 4-fold higher within the replication compartment in WT yeast than in *cdc19*$^{ts}$ yeast at the semi-permissive temperature (Figure 3D). Measuring the ATP level within the replication compartment during the course of TBSV replication revealed decreasing ATP levels when TBSV (+)repRNA synthesis became the most intensive (12-hr versus 4-hr time points, Figure 3E), indicating that the generated ATP pool in the replication compartment is efficiently used up during viral RNA replication.

To test if the high ATP accumulation within the viral replication compartment leads to altered ATP production in the cytosol, we expressed the cytosolic ATeam in yeast cells. In comparison with the virus-free yeast, expression of the p33 and p92 replication proteins decreased cytosolic ATP level by almost 2-fold, while induction of TBSV repRNA replication resulted in a ~3-fold reduction (Figure S3D). These data support the model that the increased production of ATP within the tombusvirus replication compartment is happening at the expense of cytosolic ATP levels, leading to a reduced ATP pool for cellular pathways in the cytosol. This altered distribution of the ATP pool within the cell is likely due to the recruitment of a large fraction of PK/Cdc19 into the viral replication compartment from the cytosol during viral replication.

To confirm that tombusviruses also accumulate a high ATP level within the replication compartment in a plant host, we expressed ATeam-tagged p33 replication protein in *N. benthamiana* leaves. The obtained data (Figures 4A and 4B) showed the robust production of ATP within the peroxisomal replication compartment. Similar experiments with the CIRV ATeam-p36 replication protein indicated the high level of ATP production in the mitochondrial replication compartment (Figures 4C and 4D).

VIGS-based knockdown of PK expression decreased the ATP level within the peroxisomal and mitochondrial replication compartments by ~3 and ~5-fold, respectively (Figures 5A and 5B), in comparison with the non-silenced, control *N. benthamiana* plants (Figure S4). Thus, similar to the yeast data, reduction of PK expression is detrimental to the ATP pool present within the replication compartment; this leads to reduced tombusvirus replication in plants.

## The Recruited Pyruvate Kinase Provides ATP for the Helicase Activity of Co-opted DEAD-Box Helicases in the Viral Replicase

Tombusvirus (+)RNA synthesis is affected by two groups of co-opted DEAD-box helicases (Chuang et al., 2015; Kovalev et al., 2012a; Kovalev and Nagy, 2014; Kovalev et al., 2012b). The DDX3-like Ded1p is involved in opening the promoter region in the dsRNA replication intermediate, while the eIF4IIIA-like RH2 or DDX5-like RH5 open up the replication enhancer region. To test if the co-opted PK/Cdc19 could provide the ATP requirement for these co-opted helicases, we used *in vitro* dsRNA unwinding assays (Figure 6A). We found that the CFE prepared from *cdc19*$^{ts}$ yeast could not support the efficient unwinding of the partial dsRNA duplex *in vitro*, contrary to the CFE obtained from WT yeast (Figure 6B, lane 3 versus lane 1). Addition of excess ATP to these CFEs facilitated the unwinding of the partial dsRNA (Figure 6B, lane 4), confirming that the CFEs contain the functional helicases in both WT and *cdc19*$^{ts}$ yeasts. Moreover, addition of purified GST-Cdc19 in combination with PEP and ADP substrates to the CFE from *cdc19*$^{ts}$ yeast promoted the unwinding reaction by ~10-fold (Figure 6B, lanes 10 and 11). Also, the combination of purified GST-Ded1 helicase and GST-Cdc19 in the presence of PEP substrate led to efficient unwinding of the partial dsRNA template (Figure 6C, lanes 12 and 13), further supporting the model that PK/Cdc19 could supply ATP for the co-opted DEAD-box helicases involved in TBSV (+)RNA synthesis. Similar stimulation of RH2 DEAD-box helicase function on the partial dsRNA template was observed when purified Cdc19p was added in combination with PEP substrate to either the CFE from *cdc19*$^{ts}$ yeast or the purified AtRH2 in the dsRNA unwinding assay (Figure S5).

## The Central Role of Rpn11p Deubiquitinase in Recruitment of Pyruvate Kinase into the Tombusvirus Replicase Complex

Rpn11 deubiquitinase/metalloprotease, a master regulator of many cellular processes, is co-opted by TBSV into the viral replicase (Prasanth et al., 2015). Rpn11p facilitates the recruitment of Ded1p helicase into TBSV replication, thus acting as a central organizer during the tombusvirus replicase assembly. Interestingly, Rpn11p physically interacts with Cdc19p in yeast (Guerrero et al., 2008). To analyze if Rpn11 might also affect the subversion of PK/Cdc19 into the viral replicase, we purified the replicase complex from WT and *rpn11-8*$^{ts}$ and *rpn11-14*$^{ts}$ yeasts. Interestingly, the co-purified Cdc19p was present in a reduced amount and below detection level in the replicase preparations obtained from *rpn11-8*$^{ts}$ (Figure 7A, lane 5 versus lane 6) and *rpn11-14*$^{ts}$ yeasts (Figure 7B, lane 3 versus lane 4) grown at semi-permissive temperature, respectively, in comparison with the Cdc19p level in the affinity-purified replicase preparations from WT yeast. Also, over-expression of Cdc19p in *rpn11-8*$^{ts}$ did not complement the defect in TBSV repRNA replication when grown at semi-permissive temperature (Figure S6). Further

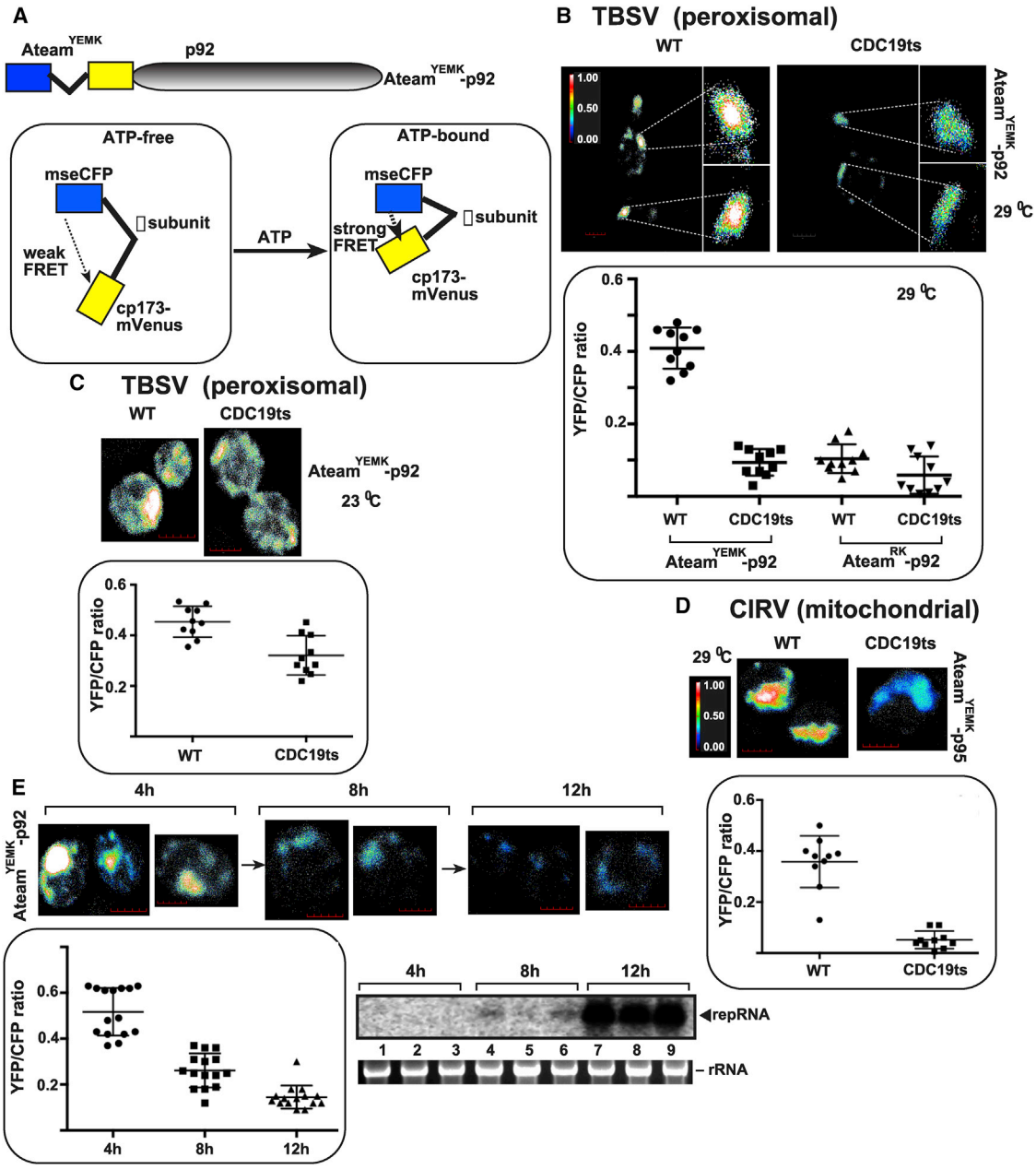


**Figure 3. The Co-opted Cytosolic Pyruvate Kinase Affects ATP Accumulation within the Tombusvirus Replication Compartment in Yeast**

(A) A scheme of FRET-based detection of ATP within the tombusvirus replication compartment. The enhanced ATP biosensor, ATeam$^{YEMK}$ was fused to TBSV p92$^{pol}$ replication protein. See further details in the Results.

(B) Comparison of the ATP level in the tombusvirus replication compartment in WT and *cdc19*$^{ts}$ yeasts grown at semi-permissive temperature using ATeam$^{YEMK}$ -p92$^{pol}$. The more intense FRET signals are white and red (between 0.5 to 1.0 ratio), whereas the low FRET signals (0.1 and below) are light blue and dark blue. We also show the quantitative FRET values (obtained with ImageJ) for a number of samples in the graph. Note that we also used a reduced ATP-sensitive version of ATeam$^{RK}$-p92 (see Figure S2) to demonstrate that the FRET signal is due to ATP-sensing, not due to p92-induced refolding of the ATeam module.

(C) Comparison of the ATP level in the tombusvirus replication compartment in WT and *cdc19*$^{ts}$ yeasts grown at permissive temperature using ATeam$^{YEMK}$ -p92$^{pol}$. See further details in (B).

(D) Comparison of the ATP level in the CIRV-induced mitochondrial replication compartment in WT and *cdc19*$^{ts}$ yeasts grown at semi-permissive temperature using ATeam$^{YEMK}$ -p95$^{pol}$. See further details in (B).

(E) Decreasing level of ATP in the TBSV replication compartment during viral replication. Top images: the FRET images were taken at different time points of TBSV repRNA replication in WT yeast expressing ATeam$^{YEMK}$ -p92$^{pol}$, as shown. See further details in (B). Bottom images: northern blot shows the accumulation of TBSV repRNA at the shown time point.

All + and − values denote standard deviation.

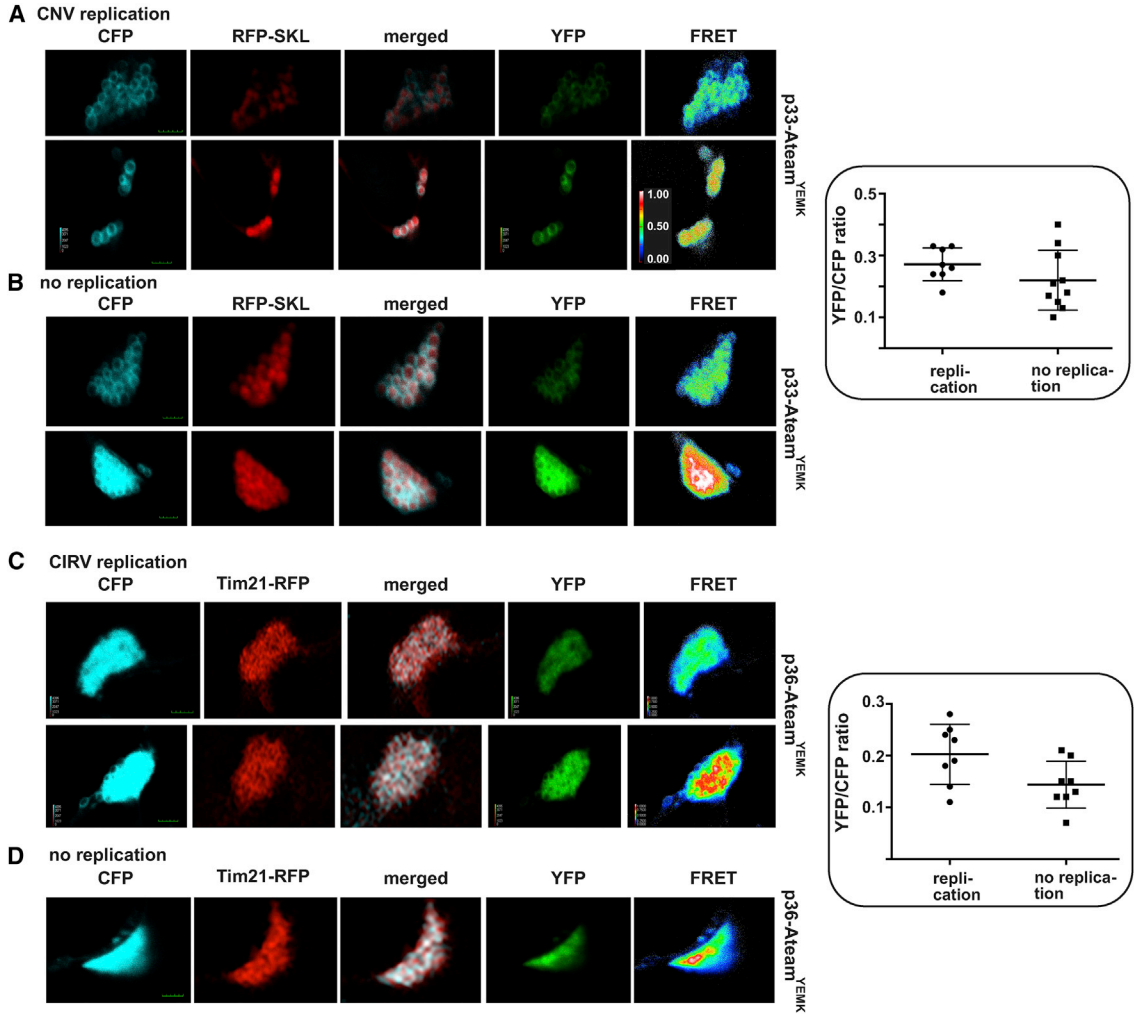


**Figure 4. ATP Accumulates to High Level within the Tombusvirus Replication Compartment in *N. benthamiana***

(A and B) Co-expression of p33-ATeam$^{YEMK}$ and RFP-SKL (peroxisomal luminar marker) was done in *N. benthamiana* leaves by agroinfiltration. The CFP signal indicates the distribution of p33-ATeam$^{YEMK}$, which co-localizes with RFP-SKL to the aggregated peroxisomes. The FRET signal is shown on the right. Shown are *N. benthamiana* cells, which are (A) infected with peroxisomal-replicating CNV or (B) mock inoculated. We show two panels to demonstrate the range of variation in FRET signals, likely due to the non-synchronous nature of infection of leaf cells.

(C and D) Comparable experiments in *N. benthamiana* using the mitochondrial CIRV p36 replication protein tagged with ATeam$^{YEMK}$ and Tim21-RFP mitochondrial marker protein. The Tim21-RFP visualized structures represent the CIRV replication protein-induced large replication compartment, consisting of aggregated mitochondria. Shown are *N. benthamiana* cells, which are (C) infected with mitochondria-replicating CIRV or (D) mock inoculated.

All + and − values denote standard deviation.

support for the central role of Rpn11p in subversion of the ATP-generating Cdc19p into the replication compartment was obtained with ATeam-p92, which showed ~4-fold and ~2-fold reduction in ATP level in *rpn11-8*$^{ts}$ and in *rpn11-14*$^{ts}$ yeasts, respectively, versus WT yeast when grown at semi-permissive temperature (Figures 7C, 7D, and S7A). Importantly, *rpn11-8*$^{ts}$ yeast showed a comparable cytosolic ATP level to that found in WT yeast when grown at both permissive and semi-permissive temperatures (Figures S7B and S7C), suggesting a near-normal level of ATP generation. Therefore, these data suggest selective defect and reduction in PK/cdc19 recruitment and, consequently, reduced ATP generation within the replication compartment in *rpn11*$^{ts}$ yeasts when they are grown at semi-permissive temperature.

## DISCUSSION

TBSV replication is an amazingly efficient process that leads to the production of vast amounts of progeny viruses in a short time period in infected cells (Nagy, 2016; Nagy and Pogany, 2011; Xu and Nagy, 2014). The robust TBSV replication likely depends on consumption of a large amount of ATP, which the virus has to obtain from the infected cell. In this work, we show evidence that TBSV co-opts glycolytic PK/Cdc19 to produce a large amount of ATP locally within the tombusviral replication compartment. Accordingly, the yeast Cdc19p and the homologous plant PK are re-targeted into the viral replication compartment in yeast and plant cells (Figure 1). This leads to the generation of ATP within the viral replication compartment, as shown

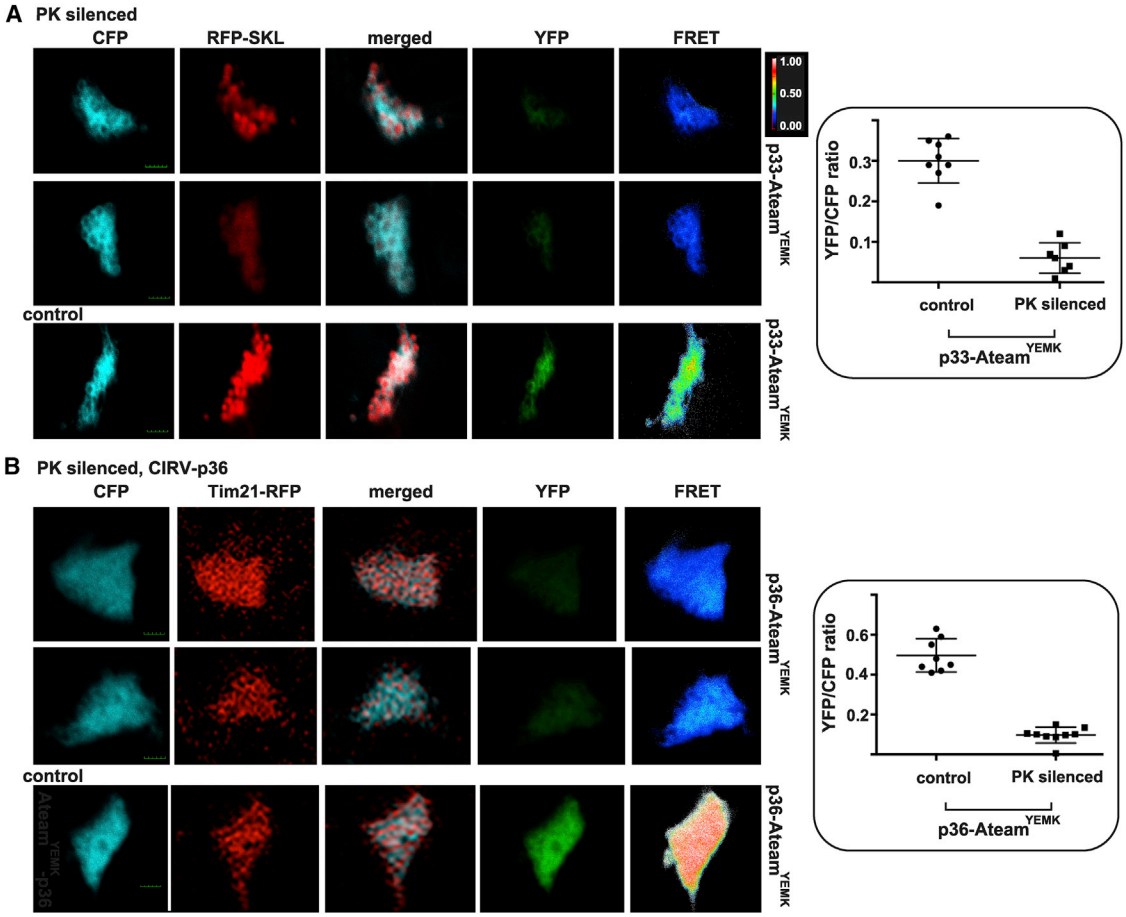


**Figure 5. Knockdown of Pyruvate Kinase Level Reduces ATP Accumulation within the Tombusvirus Replication Compartment in *N. benthamiana***

(A) VIGS-based knockdown of Nb*PK* mRNA level in *N. benthamiana* was done as in Figure 2G. Twelve days later, co-expression of p33-ATeam$^{YEMK}$ and RFP-SKL (peroxisomal luminar marker) was done in upper *N. benthamiana* leaves by agroinfiltration. The FRET signal is shown on the right. The top panels show the PK-silenced plants, whereas the lower panel shows the images obtained with the non-silenced plants. We also show the quantitative FRET values (obtained with ImageJ) for a number of samples in the graph.

(B) Comparable experiments with *PK* knockdown *N. benthamiana* using the mitochondrial CIRV p36 replication protein tagged with ATeam$^{YEMK}$ and Tim21-RFP mitochondrial marker protein. See further details in (A).

All + and − values denote standard deviation.

with the help of an ATP biosensor (Figures 3, 4, and 5). This rich ATP pool is used up during replication, as shown in a time-course experiment (Figure 3E). Using *cdc19*$^{ts}$ mutant yeast, PK gene silencing in plants and over-expression experiments, we have demonstrated a major pro-viral function of the co-opted PK/Cdc19. The co-opted PK functions in promoting efficient production of (+)RNA progeny, whereas PK does not seem to be involved in (−)RNA production, the assembly of the viral replicase, or the formation of the viral replication compartment to a great extent. In summary, we propose that the major ATP-generating component of the glycolytic pathway is hijacked by tombusviruses to support robust viral replication.

Our data is compatible with the model that PK/Cdc19 is recruited into the viral replication compartment to generate ATP locally for viral replication functions. First, PK/Cdc19 is a soluble protein, yet it was detected in the viral replicase purified from the membrane fraction (Figure 1), suggesting that PK/Cdc19 is recruited into the membrane-bound viral replicase. In addition, results obtained with Rpn11-8$^{ts}$ yeast showed that recruitment of Cdc19p was reduced into the viral replicase at semi-permissive temperature (Figure 7A), and the ATP production within the replication compartment was greatly diminished. However, the ATP production in the cytosol was comparable in Rpn11-8$^{ts}$ and WT yeasts (Figures S7B and S7C). These data are in strong agreement with the model that PK/Cdc19 produces ATP within the replication compartment and that the role of ATP diffusion from the cytosol to the replication compartment is somewhat limited.

Mechanistic studies revealed that the co-opted PK/Cdc19 provides ATP for the helicase function of subverted cellular DEAD-box helicases, which are part of the viral replicase complex (Chuang et al., 2015; Kovalev and Nagy, 2014; Kovalev et al., 2012b). These co-opted helicases are important to open up portions of the dsRNA replication intermediates to facilitate

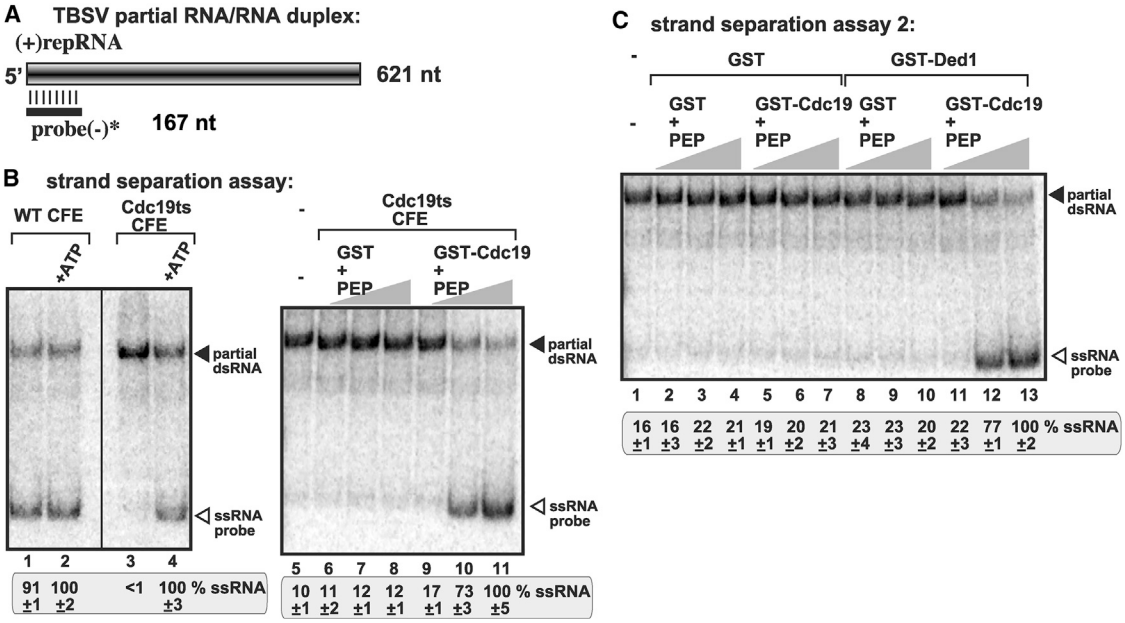


**Figure 6. PK/Cdc19 Facilitates Unwinding of Short Partial RNA/RNA Duplex by Ded1 DEAD-Box Helicase *In Vitro***

(A) Schematic representation of the partial RNA/RNA duplex used in the strand separation assay. The unlabeled template consists of DI-72 (+)repRNA and a short complementary (−)RNA (representing RI in DI-72) that anneals to the 621 nt DI-72 (+)repRNA and forms a 167 nt duplex, as shown.

(B) Representative native gel of $^{32}$P-labeled RNA products after the *in vitro* strand separation assay based on yeast CFEs prepared from WT and *cdc19*$^{ts}$ yeasts grown at semi-permissive temperature. Additional ATP (1 mM) was added to samples shown in lanes 2 and 4. Also, increasing amounts of PEP in combination with purified recombinant GST-Cdc19 and ADP were added to samples shown in lanes 9–11. Quantification of the ssRNA probe was done with a Phosphorimager. This experiment was repeated two times.

(C) Representative native gel of $^{32}$P-labeled RNA products after the *in vitro* strand separation assay based on purified recombinant GST-Ded1 DEAD-box helicase. This assay contained only the shown purified components (no CFEs added). See further details in (B).

All + and − values denote standard deviation.

(+)RNA synthesis, which is far more robust than (−)RNA synthesis (Kovalev et al., 2014). Accordingly, reduced production of new (+)repRNA is detected in *cdc19*$^{ts}$ yeast or in CFEs obtained from *cdc19*$^{ts}$ yeast (Figure 2). Based on these data, we propose that the ATP generated by the co-opted PK/Cdc19 is used to fuel subverted RNA helicases and thus to promote viral (+)RNA synthesis.

TBSV co-opts other ATP-dependent proteins, including Hsp70 molecular chaperone and Vps4p AAA+ ATPase, into the viral replicase complex (Barajas et al., 2014a; Pogany et al., 2008). These co-opted cellular ATPase proteins, however, are needed during the assembly of the viral replicase complex. Thus, inhibition of the activities of Hsp70 or Vps4p would also lead to decreased (−)RNA synthesis, which depends on correct and efficient replicase assembly (Pogany et al., 2008). The (−)RNA level, however, seems to be minimally affected in *cdc19*$^{ts}$ yeast or *in vitro* when CFEs obtained from *cdc19*$^{ts}$ were used to reconstitute the viral replicase (Figure 2). Therefore, the ATP generated by PK/Cdc19 does not seem to be utilized by these co-opted proteins for replicase assembly.

How can TBSV utilize the ATP generated by PK/Cdc19 selectively for (+)RNA synthesis? The answer, at least partially, could be the cellular Rpn11p metalloprotease, which is emerging as a critical co-opted host factor (Prasanth et al., 2015). Rpn11p mostly affects (+)RNA synthesis, and it is required for the subversion of both Cdc19p (this work) and Ded1p RNA helicase into the viral replicase complex (Prasanth et al., 2015). Therefore, we propose that the co-opted Rpn11p might regulate or restrict the availability of Cdc19p in order to channel the ATP production only for the most intensive (+)RNA synthesis step (Figure 7E). Indeed, the co-opted PK/Cdc19p is a permanent component of the replicase complex (Figure 1), indicating that PK might be able to provide ATP for an extended period needed for robust (+)RNA synthesis. Altogether, the emerging picture from our data is that PK/Cdc19p is likely recruited into the viral replicase as a protein complex also containing p33 and p92$^{pol}$ replication proteins, the co-opted Rpn11p deubiquitinase, and Ded1p helicase in yeast (Figure 7E). A similar mechanism involving the viral replication proteins Rpn11 and RH2 DEAD-box helicase might exist in plants.

The advantage of co-opting PK/Cdc19 to the replicase complex is that the virus replication machinery does not need to intensively compete with cellular processes for access to ATP. Also, local production of ATP within the replication compartment could greatly facilitate the kinetics of RNA synthesis by providing high ATP concentration to drive co-opted RNA helicases.

Viruses are known to take advantage of the reprogramming of the glycolytic pathway during infections (Findlay and Ulaeto, 2015; Su et al., 2014). For example, Dengue virus, a cytosolic (+)RNA virus, upregulates glucose consumption by enhancing the expression of both glucose transporter 1 and hexokinase 2 (Fontaine et al., 2015). Hepatitis C virus accumulates ATP at

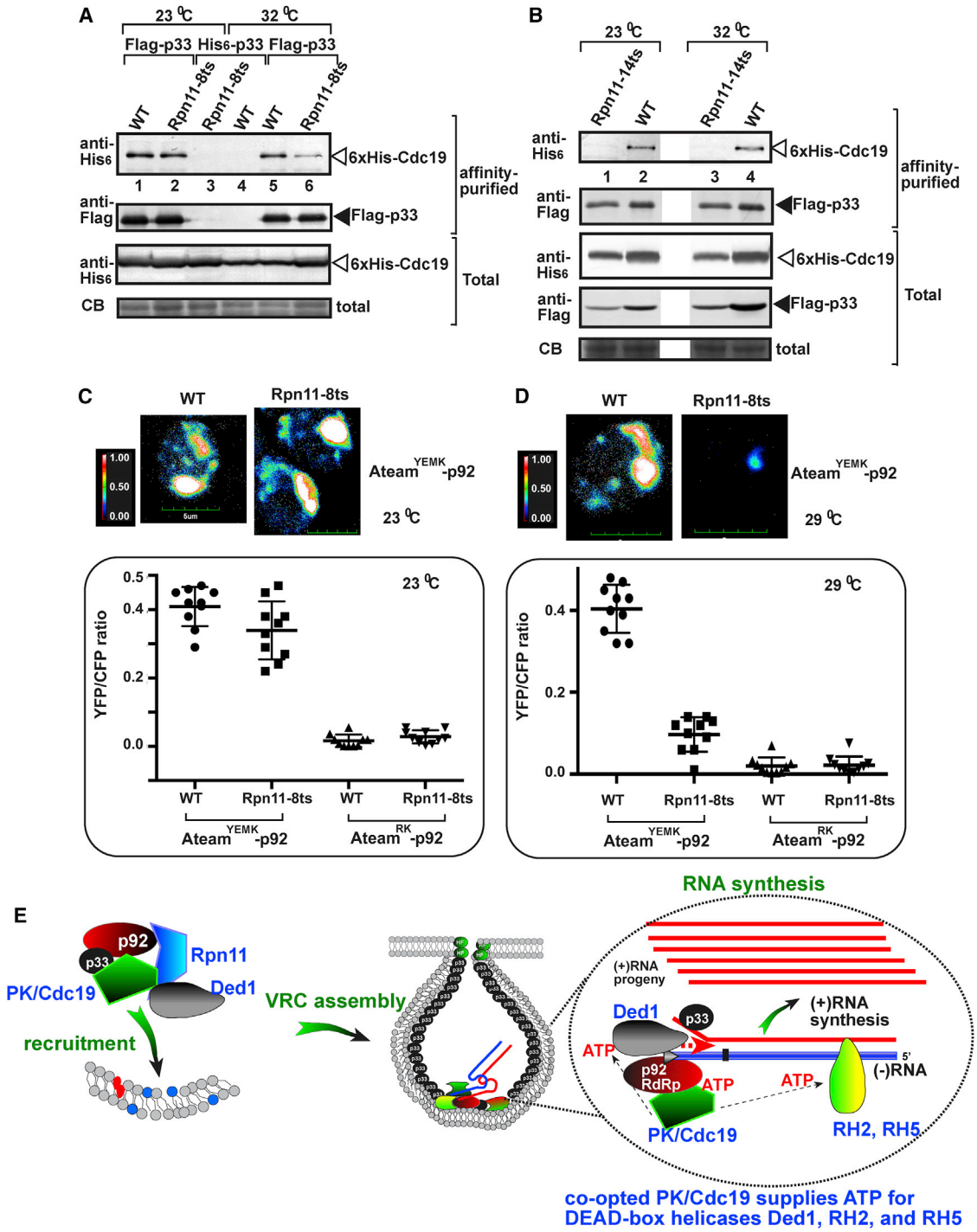


**Figure 7. The Role of the Co-opted Rpn11 Deubiquitinase in Recruitment of the Cytosolic Pyruvate Kinase into the Viral Replicase**

(A) Co-purification of the yeast Cdc19p with the viral replicase complex from WT and *rpn11-8*$^{ts}$ and *rpn11-14*$^{ts}$ yeasts grown at permissive and semi-permissive temperatures. Top panel: western blot analysis of co-purified $His_6$-Cdc19 with FLAG-affinity purified p33 and FLAG-p92$^{pol}$ from yeast membrane fraction. Cdc19p was detected by western blot with anti-His antibody. Second panel: western blot analysis of FLAG-affinity-purified p33 from yeast membrane fractions. Bottom three panels: western blots of $His_6$-Cdc19 and FLAG-p33 in total protein extracts detected with anti-His and anti-FLAG antibodies, respectively. The Coomassie-blue-stained SDS-PAGE gel of total protein extracts is shown at the bottom.

(B) Co-purification of the yeast Cdc19p with the viral replicase complex from WT and *rpn11-14*$^{ts}$ yeasts grown at permissive and semi-permissive temperatures. See further details in (A).

(C) Comparison of the ATP levels in the tombusvirus replication compartment in WT and *rpn11-8*$^{ts}$ yeasts grown at permissive temperature using ATeam$^{YEMK}$ -p92$^{pol}$. See further details in Figure 3B.

*(legend continued on next page)*

the site of virus replication, which is likely to fuel various viral processes (Ando et al., 2012). Therefore, it is possible that metabolic reprogramming of the glycolytic pathway and recruitment of cytosolic glycolytic enzymes into the viral replication compartment to fulfill the energy demands of viruses is a widespread phenomenon during various viral infections.

## STAR★METHODS

Detailed methods are provided in the online version of this paper and include the following:

- KEY RESOURCES TABLE
- CONTACT FOR REAGENT AND RESOURCE SHARING
- EXPERIMENTAL MODEL AND SUBJECT DETAILS
  - Yeast Strains and Expression Plasmids
  - Plant Expression Plasmids
- METHOD DETAILS
  - Yeast Transformation and Cultivation
  - Virus Strains and Plant Infections
  - Tombusvirus RNA Analysis
  - VIGS-based Knockdown of Pyruvate Kinase in *N. benthamiana* Plants
  - Yeast Cell Free Extract (CFE) Based In Vitro Replication Assay
  - Flag-affinity Purification of Tombusvirus Replicase from Yeast and In Vitro RdRp Assay
  - Co-purification of Cdc19p with the Tombusvirus Replication Complex
  - Recombinant Protein Purification from *E coli*
  - Recombinant Protein Purification from Yeast
  - Cdc19 Pull-down Assay
  - dsRNA Strand Separation Assay
  - Confocal Microscopic Analysis of Yeast Cells
  - Co-localization and Bimolecular Fluorescence Complementation Assay in *planta*
  - Visualization and Measurement of ATP Levels in Yeast
  - Visualization and Measurement of ATP Levels in Plants
- QUANTIFICATION AND STATISTICAL ANALYSIS

## SUPPLEMENTAL INFORMATION

Supplemental Information includes seven figures and one table and can be found with this article online at https://doi.org/10.1016/j.chom.2017.10.004.

## AUTHOR CONTRIBUTIONS

C.C., K.R.P., and P.D.N. conceived and designed the experiments. C.C. and K.R.P. performed the experiments. C.C., K.R.P., and P.D.N. wrote the manuscript.

## ACKNOWLEDGEMENTS

We thank Dr. Judit Pogany for comments on the manuscript. The temperature-sensitive yeast strains *cdc19$^{ts}$*, *rpn11-8$^{ts}$*, and *rpn11-14$^{ts}$* were a generous gift from Dr. C. Boone (U. Toronto). The authors thank Drs. H. Imamura and H. Noji for providing plasmids pRSET-ATeam$^{YEMK}$ and pRSET-ATeam$^{RK}$. This work was supported by NSF-MCB (1517751).

Received: February 17, 2017
Revised: July 24, 2017
Accepted: October 3, 2017
Published: October 26, 2017

## REFERENCES

Ando, T., Imamura, H., Suzuki, R., Aizaki, H., Watanabe, T., Wakita, T., and Suzuki, T. (2012). Visualization and measurement of ATP levels in living cells replicating hepatitis C virus genome RNA. PLoS Pathog. *8*, e1002561.

Barajas, D., Jiang, Y., and Nagy, P.D. (2009a). A unique role for the host ESCRT proteins in replication of Tomato bushy stunt virus. PLoS Pathog. *5*, e1000705.

Barajas, D., Li, Z., and Nagy, P.D. (2009b). The Nedd4-type Rsp5p ubiquitin ligase inhibits tombusvirus replication by regulating degradation of the p92 replication protein and decreasing the activity of the tombusvirus replicase. J. Virol. *83*, 11751–11764.

Barajas, D., Martín, I.F., Pogany, J., Risco, C., and Nagy, P.D. (2014a). Noncanonical role for the host Vps4 AAA+ ATPase ESCRT protein in the formation of Tomato bushy stunt virus replicase. PLoS Pathog. *10*, e1004087.

Barajas, D., Xu, K., de Castro Martín, I.F., Sasvari, Z., Brandizzi, F., Risco, C., and Nagy, P.D. (2014b). Co-opted oxysterol-binding ORP and VAP proteins channel sterols to RNA virus replication sites via membrane contact sites. PLoS Pathog. *10*, e1004388.

Burgyan, J., Rubino, L., and Russo, M. (1996). The 5′-terminal region of a tombusvirus genome determines the origin of multivesicular bodies. J. Gen. Virol. *77*, 1967–1974.

Chuang, C., Barajas, D., Qin, J., and Nagy, P.D. (2014). Inactivation of the host lipin gene accelerates RNA virus replication through viral exploitation of the expanded endoplasmic reticulum membrane. PLoS Pathog. *10*, e1003944.

Chuang, C., Prasanth, K.R., and Nagy, P.D. (2015). Coordinated function of cellular DEAD-box helicases in suppression of viral RNA recombination and maintenance of viral genome integrity. PLoS Pathog. *11*, e1004680.

den Boon, J.A., and Ahlquist, P. (2010). Organelle-like membrane compartmentalization of positive-strand RNA virus replication factories. Annu. Rev. Microbiol. *64*, 241–256.

Diamond, D.L., Syder, A.J., Jacobs, J.M., Sorensen, C.M., Walters, K.A., Proll, S.C., McDermott, J.E., Gritsenko, M.A., Zhang, Q., Zhao, R., et al. (2010). Temporal proteome and lipidome profiles reveal hepatitis C virus-associated reprogramming of hepatocellular metabolism and bioenergetics. PLoS Pathog. *6*, e1000719.

Dinesh-Kumar, S.P., Anandalakshmi, R., Marathe, R., Schiff, M., and Liu, Y. (2003). Virus-induced gene silencing. Methods Mol. Biol. *236*, 287–294.

Fernández de Castro, I., Tenorio, R., and Risco, C. (2016). Virus assembly factories in a lipid world. Curr. Opin. Virol. *18*, 20–26.

(D) Comparison of the ATP levels in the tombusvirus replication compartment in WT and *rpn11-8$^{ts}$* yeasts grown at semi-permissive temperature using ATeam$^{YEMK}$ -p92$^{pol}$.

(E) A model on the role of the co-opted glycolytic PK/Cdc19 in tombusvirus replication. Direct interaction of the cytosolic PK/Cdc19 with the viral p33 and p92$^{pol}$ replication proteins, in combination with interaction of PK/Cdc19 with the cellular Rpn11p—which also interacts with p33 and p92$^{pol}$ replication proteins and the cellular Ded1 DEAD-box helicase—leads to recruitment of PK/Cdc19 into the membranous replication compartment. After VRC assembly and (−)RNA synthesis (not shown in detail here), PK/Cdc19 generates ATP to fuel the dsRNA unwinding function of the co-opted cellular DDX3-like Ded1, DDX5-like RH5, and the eIF4AIII-like RH2 DEAD-box helicases on dsRNA replication intermediate. These activities in the VRC lead to the production of an excess amount of (+)RNA progeny, which is then released from VRC. The co-opted PK/Cdc19 is a permanent component of the active viral replicase complex.
All + and − values denote standard deviation.

Fernández de Castro, I., Fernandez, J.J., Barajas, D., Nagy, P.D., and Risco, C. (2017). Three dimensional imaging of the intracellular assembly of a functional viral RNA replicase complex. J. Cell Sci. *130*, 260–268.

Findlay, J.S., and Ulaeto, D. (2015). Semliki Forest virus and Sindbis virus, but not vaccinia virus, require glycolysis for optimal replication. J. Gen. Virol. *96*, 2693–2696.

Fontaine, K.A., Sanchez, E.L., Camarda, R., and Lagunoff, M. (2015). Dengue virus induces and requires glycolysis for optimal replication. J. Virol. *89*, 2358–2366.

Goodin, M.M., Dietzgen, R.G., Schichnes, D., Ruzin, S., and Jackson, A.O. (2002). pGD vectors: versatile tools for the expression of green and red fluorescent protein fusions in agroinfiltrated plant leaves. Plant J. *31*, 375–383.

Guerrero, C., Milenkovic, T., Przulj, N., Kaiser, P., and Huang, L. (2008). Characterization of the proteasome interaction network using a QTAX-based tag-team strategy and protein interaction network analysis. Proc. Natl. Acad. Sci. USA *105*, 13333–13338.

Hearne, P.Q., Knorr, D.A., Hillman, B.I., and Morris, T.J. (1990). The complete genome structure and synthesis of infectious RNA from clones of tomato bushy stunt virus. Virology *177*, 141–151.

Huang, T.S., and Nagy, P.D. (2011). Direct inhibition of tombusvirus plus-strand RNA synthesis by a dominant negative mutant of a host metabolic enzyme, glyceraldehyde-3-phosphate dehydrogenase, in yeast and plants. J. Virol. *85*, 9090–9102.

Imamura, H., Nhat, K.P., Togawa, H., Saito, K., Iino, R., Kato-Yamada, Y., Nagai, T., and Noji, H. (2009). Visualization of ATP levels inside single living cells with fluorescence resonance energy transfer-based genetically encoded indicators. Proc. Natl. Acad. Sci. USA *106*, 15651–15656.

Jaag, H.M., and Nagy, P.D. (2009). Silencing of Nicotiana benthamiana Xrn4p exoribonuclease promotes tombusvirus RNA accumulation and recombination. Virology *386*, 344–352.

Jiang, Y., Serviene, E., Gal, J., Panavas, T., and Nagy, P.D. (2006). Identification of essential host factors affecting tombusvirus RNA replication based on the yeast Tet promoters Hughes Collection. J. Virol. *80*, 7394–7404.

Kovalev, N., and Nagy, P.D. (2014). The expanding functions of cellular helicases: the tombusvirus RNA replication enhancer co-opts the plant eIF4AIII-like AtRH2 and the DDX5-like AtRH5 DEAD-box RNA helicases to promote viral asymmetric RNA replication. PLoS Pathog. *10*, e1004051.

Kovalev, N., Barajas, D., and Nagy, P.D. (2012a). Similar roles for yeast Dbp2 and Arabidopsis RH20 DEAD-box RNA helicases to Ded1 helicase in tombusvirus plus-strand synthesis. Virology *432*, 470–484.

Kovalev, N., Pogany, J., and Nagy, P.D. (2012b). A Co-opted DEAD-box RNA helicase enhances tombusvirus plus-strand synthesis. PLoS Pathog. *8*, e1002537.

Kovalev, N., Pogany, J., and Nagy, P.D. (2014). Template role of double-stranded RNA in tombusvirus replication. J. Virol. *88*, 5638–5651.

Li, Z., Barajas, D., Panavas, T., Herbst, D.A., and Nagy, P.D. (2008). Cdc34p ubiquitin-conjugating enzyme is a component of the tombusvirus replicase complex and ubiquitinates p33 replication protein. J. Virol. *82*, 6911–6926.

Li, Z., Pogany, J., Tupman, S., Esposito, A.M., Kinzy, T.G., and Nagy, P.D. (2010). Translation elongation factor 1A facilitates the assembly of the tombusvirus replicase and stimulates minus-strand synthesis. PLoS Pathog. *6*, e1001175.

Li, Z., Vizeacoumar, F.J., Bahr, S., Li, J., Warringer, J., Vizeacoumar, F.S., Min, R., Vandersluis, B., Bellay, J., Devit, M., et al. (2011). Systematic exploration of essential yeast gene function with temperature-sensitive mutants. Nat. Biotechnol. *29*, 361–367.

Nagy, P.D. (2008). Yeast as a model host to explore plant virus-host interactions. Annu. Rev. Phytopathol. *46*, 217–242.

Nagy, P.D. (2016). Tombusvirus-Host Interactions: Co-opted evolutionarily conserved host factors take center court. Annu. Rev. Virol. *3*, 491–515.

Nagy, P.D., and Pogany, J. (2011). The dependence of viral RNA replication on co-opted host factors. Nat. Rev. Microbiol. *10*, 137–149.

Nawaz-ul-Rehman, M.S., Reddisiva Prasanth, K., Baker, J., and Nagy, P.D. (2013). Yeast screens for host factors in positive-strand RNA virus replication based on a library of temperature-sensitive mutants. Methods *59*, 207–216.

Nawaz-ul-Rehman, M.S., Prasanth, K.R., Xu, K., Sasvari, Z., Kovalev, N., de Castro Martín, I.F., Barajas, D., Risco, C., and Nagy, P.D. (2016). Viral replication protein inhibits cellular cofilin actin depolymerization factor to regulate the actin network and promote viral replicase assembly. PLoS Pathog. *12*, e1005440.

Panavas, T., and Nagy, P.D. (2003). Yeast as a model host to study replication and recombination of defective interfering RNA of Tomato bushy stunt virus. Virology *314*, 315–325.

Panavas, T., Hawkins, C.M., Panaviene, Z., and Nagy, P.D. (2005a). The role of the p33:p33/p92 interaction domain in RNA replication and intracellular localization of p33 and p92 proteins of Cucumber necrosis tombusvirus. Virology *338*, 81–95.

Panavas, T., Serviene, E., Brasher, J., and Nagy, P.D. (2005b). Yeast genome-wide screen reveals dissimilar sets of host genes affecting replication of RNA viruses. Proc. Natl. Acad. Sci. USA *102*, 7326–7331.

Panavas, T., Serviene, E., Pogany, J., and Nagy, P.D. (2008). Genome-wide screens for identification of host factors in viral replication. Methods Mol. Biol. *451*, 615–624.

Panaviene, Z., Baker, J.M., and Nagy, P.D. (2003). The overlapping RNA-binding domains of p33 and p92 replicase proteins are essential for tombusvirus replication. Virology *308*, 191–205.

Panaviene, Z., Panavas, T., Serva, S., and Nagy, P.D. (2004). Purification of the cucumber necrosis virus replicase from yeast cells: role of coexpressed viral RNA in stimulation of replicase activity. J. Virol. *78*, 8254–8263.

Paul, D., and Bartenschlager, R. (2015). Flaviviridae replication organelles: oh, what a tangled web we weave. Annu. Rev. Virol. *2*, 289–310.

Peng, M., Yin, N., Chhangawala, S., Xu, K., Leslie, C.S., and Li, M.O. (2016). Aerobic glycolysis promotes T helper 1 cell differentiation through an epigenetic mechanism. Science *354*, 481–484.

Pogany, J., and Nagy, P.D. (2008). Authentic replication and recombination of Tomato bushy stunt virus RNA in a cell-free extract from yeast. J. Virol. *82*, 5967–5980.

Pogany, J., and Nagy, P.D. (2012). p33-Independent activation of a truncated p92 RNA-dependent RNA polymerase of Tomato bushy stunt virus in yeast cell-free extract. J. Virol. *86*, 12025–12038.

Pogany, J., Stork, J., Li, Z., and Nagy, P.D. (2008). In vitro assembly of the Tomato bushy stunt virus replicase requires the host Heat shock protein 70. Proc. Natl. Acad. Sci. USA *105*, 19956–19961.

Prasanth, K.R., Barajas, D., and Nagy, P.D. (2015). The proteasomal Rpn11 metalloprotease suppresses tombusvirus RNA recombination and promotes viral replication via facilitating assembly of the viral replicase complex. J. Virol. *89*, 2750–2763.

Rajendran, K.S., and Nagy, P.D. (2003). Characterization of the RNA-binding domains in the replicase proteins of tomato bushy stunt virus. J. Virol. *77*, 9244–9258.

Rajendran, K.S., and Nagy, P.D. (2006). Kinetics and functional studies on interaction between the replicase proteins of Tomato Bushy Stunt Virus: requirement of p33:p92 interaction for replicase assembly. Virology *345*, 270–279.

Rochon, D.M., and Johnston, J.C. (1991). Infectious transcripts from cloned cucumber necrosis virus cDNA: evidence for a bifunctional subgenomic mRNA. Virology *181*, 656–665.

Rochon, D., Singh, B., Reade, R., Theilmann, J., Ghoshal, K., Alam, S.B., and Maghodia, A. (2014). The p33 auxiliary replicase protein of Cucumber necrosis virus targets peroxisomes and infection induces de novo peroxisome formation from the endoplasmic reticulum. Virology *452-453*, 133–142.

Sasvari, Z., Izotova, L., Kinzy, T.G., and Nagy, P.D. (2011). Synergistic roles of eukaryotic translation elongation factors 1Bγ and 1A in stimulation of tombusvirus minus-strand synthesis. PLoS Pathog. *7*, e1002438.

Serva, S., and Nagy, P.D. (2006). Proteomics analysis of the tombusvirus replicase: Hsp70 molecular chaperone is associated with the replicase and enhances viral RNA replication. J. Virol. *80*, 2162–2169.

Sopko, R., Huang, D., Preston, N., Chua, G., Papp, B., Kafadar, K., Snyder, M., Oliver, S.G., Cyert, M., Hughes, T.R., et al. (2006). Mapping pathways and phenotypes by systematic gene overexpression. Mol. Cell *21*, 319–330.

Stine, Z.E., and Dang, C.V. (2013). Stress eating and tuning out: cancer cells re-wire metabolism to counter stress. Crit. Rev. Biochem. Mol. Biol. *48*, 609–619.

Su, M.A., Huang, Y.T., Chen, I.T., Lee, D.Y., Hsieh, Y.C., Li, C.Y., Ng, T.H., Liang, S.Y., Lin, S.Y., Huang, S.W., et al. (2014). An invertebrate Warburg effect: a shrimp virus achieves successful replication by altering the host metabolome via the PI3K-Akt-mTOR pathway. PLoS Pathog. *10*, e1004196.

Teng, C.F., Hsieh, W.C., Wu, H.C., Lin, Y.J., Tsai, H.W., Huang, W., and Su, I.J. (2015). Hepatitis B virus pre-S2 mutant induces aerobic glycolysis through mammalian target of rapamycin signal cascade. PLoS One *10*, e0122373.

Valentini, G., Chiarelli, L., Fortin, R., Speranza, M.L., Galizzi, A., and Mattevi, A. (2000). The allosteric regulation of pyruvate kinase. J. Biol. Chem. *275*, 18145–18152.

Vander Heiden, M.G., Locasale, J.W., Swanson, K.D., Sharfi, H., Heffron, G.J., Amador-Noguez, D., Christofk, H.R., Wagner, G., Rabinowitz, J.D., Asara, J.M., and Cantley, L.C. (2010). Evidence for an alternative glycolytic pathway in rapidly proliferating cells. Science *329*, 1492–1499.

Wang, A. (2015). Dissecting the molecular network of virus-plant interactions: the complex roles of host factors. Annu. Rev. Phytopathol. *53*, 45–66.

Wang, R.Y., and Nagy, P.D. (2008). Tomato bushy stunt virus co-opts the RNA-binding function of a host metabolic enzyme for viral genomic RNA synthesis. Cell Host Microbe *3*, 178–187.

Xu, K., and Nagy, P.D. (2014). Expanding use of multi-origin subcellular membranes by positive-strand RNA viruses during replication. Curr. Opin. Virol. *9*, 119–126.

Xu, K., and Nagy, P.D. (2016). Enrichment of phosphatidylethanolamine in viral replication compartments via co-opting the endosomal Rab5 small GTPase by a positive-strand RNA virus. PLoS Biol. *14*, e2000128.

Xu, K., Huang, T.S., and Nagy, P.D. (2012). Authentic in vitro replication of two tombusviruses in isolated mitochondrial and endoplasmic reticulum membranes. J. Virol. *86*, 12779–12794.

Xu, K., Lin, J.Y., and Nagy, P.D. (2014). The hop-like stress-induced protein 1 cochaperone is a novel cell-intrinsic restriction factor for mitochondrial tombusvirus replication. J. Virol. *88*, 9361–9378.

## STAR★METHODS

### KEY RESOURCES TABLE

| REAGENT or RESOURCE | SOURCE | IDENTIFIER |
|---|---|---|
| Antibodies | | |
| Monoclonal ANTI-FLAG M2 | Sigma | F1804; RRID: AB_262044 |
| Anti-His antibody | Sigma | H1029; RRID: AB_260015 |
| Bacterial and Virus Strains | | |
| Tomato bushy stunt virus, cherry strain | Dr. KA White | N/A |
| Cucumber necrosis virus | Dr. KA White | N/A |
| Carnation Italian ringspot virus, type strain | ATCC | PVMC-47 |
| E coli strain BL21 (DE3) CodonPlus | Agilent | NC9122855 |
| E. coli Top10 | Invitrogen | C4040-03 |
| Agrobacterium strain C58C1 | Dr. M. Goodin (UKY) | N/A |
| Chemicals, Peptides, and Recombinant Proteins | | |
| $^{32}$P-UTP | Perkin Elmer | BLU007H500UC |
| anti-FLAG M2 agarose | Sigma | A2220 |
| Experimental Models: Cell Lines | | |
| Nicotiana benthamiana | Wild type, lab strain | N/A |
| Experimental Models: Organisms/Strains | | |
| *Saccharomyces cerevisiae* BY4741 | Open Biosystems | YSC6273 |
| *S. cerevisiae* CDC19ts | Dr. C. Boone (U. Toronto)(Li et al., 2011) | N/A |
| *S. cerevisiae* RPN11-8ts | Dr. C. Boone (U. Toronto)(Li et al., 2011) | N/A |
| *S. cerevisiae* RPN11-14ts | Dr. C. Boone (U. Toronto)(Li et al., 2011) | N/A |
| Nicotiana benthamiana | Wild type | N/A |
| Oligonucleotides | | |
| Table S1 | This paper | N/A |
| Recombinant DNA | | |
| Plasmid: LpGAD-CUP1::HisFlag-p92 (*LEU2* selection) | (Li et al., 2008) | N/A |
| Plasmid: HpGBK-CUP1::HisFlag-p33/ GAL1::DI-72 (*HIS3* selection) | (Barajas et al., 2009b) | N/A |
| Plasmid: UpYC-GAL1::DI-72 (*URA3* selection) | (Panaviene et al., 2004) | N/A |
| Plasmid: HpGBK-CUP1::His-p33/ GAL1::DI-72 (*HIS3* selection) | (Barajas et al., 2009b) | N/A |
| Plasmid: HpGBK-CUP1::Flag-p33/ GAL1::DI-72 (*HIS3* selection) | (Barajas et al., 2009b) | N/A |
| Plasmid: LpGAD-CUP1::His-p92 (*LEU2* selection) | (Barajas et al., 2009b) | N/A |
| Plasmid: LpGAD-CUP1::Flag-p92 (*LEU2* selection) | Dr. J. Pogany (U. Kentucky) | N/A |
| Plasmid: LpESC-CUP1::Flag-p95 (*LEU2* selection) | J. Pogany (U. Kentucky) | N/A |
| Plasmid: HpESC-CUP1::Flag-p36 (*HIS3* selection) | J. Pogany (U. Kentucky) | N/A |
| Plasmid: UpYES-GAL1::His-cdc19 | This paper | N/A |
| Plasmid: UpYES-GAL1::His-YFP-CDC19 | This paper | N/A |
| Plasmid: LpGAD-ADH::ATeam$^{YEMK}$ –p92 | This paper | N/A |
| Plasmid: LpGAD-ADH:: ATeam$^{RK}$ –p92 | This paper | N/A |

(*Continued on next page*)

*Continued*

| REAGENT or RESOURCE | SOURCE | IDENTIFIER |
|---|---|---|
| Plasmid: HpESC-CUP1::ATeam$^{YEMK}$-p95 | This paper | N/A |
| Plasmid: pRSET-ATeam$^{YEMK}$ | Drs. H. Imamura and H. Noji(Imamura et al., 2009) | N/A |
| Plasmid: pRSET-ATeam$^{RK}$ | Drs. H. Imamura and H. Noji(Imamura et al., 2009) | N/A |
| Plasmid: UpYES-GAL1::ATeam$^{YEMK}$ | This paper | N/A |
| Plasmid: LpGAD-ADH::NbPK | This paper | N/A |
| Plasmid: HpESC-Gal1::Flag-rsGFP | This paper | N/A |
| Plasmid: UpYES-Gal1::His-GST-CDC19$^{FL}$ | This paper | N/A |
| Plasmid: UpYES-Gal1::His-GST-CDC19$^{nt1-1080}$ | This paper | N/A |
| Plasmid: UpYES-Gal1::His-GST-CDC19$^{nt1-555}$ | This paper | N/A |
| Plasmid: UpYES-Gal1::His-GST-CDC19$^{nt268-1503}$ | This paper | N/A |
| Plasmid: pGD-35S::p92-cYFP | This paper | N/A |
| Plasmid: UpYES-T92 | (Xu et al., 2012) | N/A |
| Plasmid: pMAL-p33c | (Rajendran and Nagy, 2006) | N/A |
| Plasmid: pMAL-pC151-240 | (Rajendran and Nagy, 2006) | N/A |
| Plasmid: pMAL-pC211-296 | (Rajendran and Nagy, 2006) | N/A |
| Plasmid: pMAL-pC219-296 | (Rajendran and Nagy, 2006) | N/A |
| Plasmid: pGD-35S::p33-BFP | (Xu and Nagy, 2016) | N/A |
| Plasmid: pGD-35S::p33-cYFP | (Xu and Nagy, 2016) | N/A |
| Plasmid: pGD-35S::RFP-SKL | (Xu and Nagy, 2016) | N/A |
| Plasmid: pGD-35S::AtTim21-RFP | (Xu and Nagy, 2016) | N/A |
| Plasmid: pGD-35S::p19 | (Xu and Nagy, 2016) | N/A |
| Plasmid: pGD-NbPK | This paper | N/A |
| Plasmid: pGD-GFP-PK | This paper | N/A |
| Plasmid: pGD-nYFP-PK | This paper | N/A |
| Plasmid: pGD-p33-ATeam$^{YEMK}$ | This paper | N/A |
| Plasmid: pGD-p36-ATeam$^{YEMK}$ | This paper | N/A |
| Plasmid: pMAL-Ded1 | (Kovalev et al., 2012b) | N/A |
| Plasmid: pMAL-33 | (Rajendran and Nagy, 2003) | N/A |
| Plasmid: pMAL92 | (Rajendran and Nagy, 2003) | N/A |
| Plasmid: pTRV2-PK | This paper | N/A |
| Plasmid: GST-Cdc19 | Open biosystems | YSC4423 |
| Plasmid: TRV-cGFP | (Xu et al., 2014) | N/A |
| Software and Algorithms | | |
| Olympus FLUOVIEW 1.5 software | Olympus | N/A |
| ImageJ software | NIH | https://imagej.nih.gov/ij/ |
| Image lab 3.0 | Bio-Rad | N/A |
| ImageQuant TL | GE | N/A |

## CONTACT FOR REAGENT AND RESOURCE SHARING

Further information and requests for resources and reagents should be directed to and will be fulfilled by the Lead Contact, Peter D. Nagy (pdnagy2@uky.edu).

## EXPERIMENTAL MODEL AND SUBJECT DETAILS

### Yeast Strains and Expression Plasmids

The yeast (*Saccharomyces cerevisiae*) strain BY4741 (*MATa his3Δ1 leu2Δ0 met15Δ0 ura3Δ0*), was obtained from Open Biosystems. The temperature-sensitive (ts) yeast strains *cdc19*$^{ts}$, *rpn11-8* $^{ts}$ and *rpn11-14* $^{ts}$ were obtained from Dr. C. Boone (U. Toronto) (Li et al., 2011).

The following yeast expression plasmids have been previously described: LpGAD-CUP1::HisFlag-p92 (*LEU2* selection), HpGBK-CUP1::HisFlag-p33/GAL1::DI-72 (*HIS3* selection), LpGAD-ADH::CFP-p92 (*LEU2* selection), UpYC-GAL1::DI-72 (*URA3* selection) (Panavas et al., 2005a), HpGBK-CUP1::His-p33/GAL1::DI-72 (*HIS3* selection), HpGBK-CUP1::Flag-p33/GAL1::DI-72 (*HIS3* selection), LpGAD-CUP1::His-p92 (*LEU2* selection), LpGAD-CUP1::Flag-p92 (*LEU2* selection) (Barajas et al., 2009a), LpESC-CUP1::Flag-p95 (*LEU2* selection), HpESC-CUP1::Flag-p36 (*HIS3* selection) (J. Pogany and P.D.N., unpublished data).

To obtain plasmid UpYES-GAL1::His-cdc19 plasmid, the yeast *CDC19* ORF was PCR-amplified with primers #5992 and #5993, and then the obtained PCR product was cloned into UpYES vector at BamHI and XhoI sites. To make UpYES-GAL1::His-YFP-CDC19 plasmid, the plasmid UpYES-YFP-p92 was used as template in PCR with primers #1291 and #1295 to obtain the YFP fragment. The PCR product was cloned into UpYES-GAL1::His-cdc19 plasmid at the BamHI site. To obtain plasmids LpGAD-ADH::ATeam$^{YEMK}$ –p92, LpGAD-ADH:: ATeam$^{RK}$ –p92, HpESC-CUP1::ATeam$^{YEMK}$-p95 and HpESC-CUP1::ATeam$^{RK}$-p95, plasmids pRSET-ATeam$^{YEMK}$ and pRSET-ATeam$^{RK}$ (Imamura et al., 2009) were used as templates, respectively, in PCR with primers #3494 and #6752, and then the obtained PCR products were digested with BamHI and BglII and cloned either into BamHI-digested LpGAD-ADH::p92 or HpESC-CUP1::p95 plasmids. To make UpYES-GAL1::ATeam$^{YEMK}$ plasmid, the ATeamYEMK fragment was PCR-amplified by using plasmid pRSET-ATeam$^{YEMK}$ as a template and primers #1293 and #6794. The PCR product was cloned into UpYES vector at XhoI/XbaI sites. To generate the plasmid LpGAD-ADH::NbPK, the plant *pyruvate kinase* gene fragment was PCR-amplified from *N. benthamiana* cDNA using primers #6660 and #6661, followed by the digestion of PCR products with BamHI/SalI and then, cloned into pGAD-ADH plasmid at BamHI/XhoI sites.

To generate plasmid HpESC-Gal1::Flag-rsGFP, the plasmid pGD-35S::GFP was used as template in PCR with primers #5160 and #7104 to obtain rsGFP fragment, and then the obtained PCR product was cloned into HpESC plasmid at EcoRI/SpeI sites. To construct the plasmids for overexpression of GST tagged Cdc19 and its truncated derivatives, plasmid UpYES-GAL1::His-cdc19 was used as template in PCR reaction with primer pairs #7186 / #5993; #7186 / #7118; #7186 / #7119 and #7185 / #5993 respectively. The obtained PCR products were separately cloned into UpYES-His-GST plasmid at NotI/XhoI sites to generate UpYES-Gal1::His-GST-CDC19$^{FL}$, UpYES-Gal1::His-GST-CDC19$^{nt1\text{-}1080}$, UpYES-Gal1::His-GST-CDC19$^{nt1\text{-}555}$, UpYES-Gal1::His-GST-CDC19$^{nt268\text{-}1503}$. To generate plasmid pGD-35S::p92-cYFP, the plasmid UpYES-T92 was used as template in PCR with primer #6075 and #5838 to obtain the TBSV p92 fragment. The obtained PCR product was cloned into plasmid pGD-C-cYFP at BamHI/PstI sites. The *E. coli* expression plasmids pMAL-p33c, pMAL-pC151-240, pMAL-pC211-296, pMAL-pC219-296 were described before (Rajendran and Nagy, 2006).

### Plant Expression Plasmids

The plants expression plasmids pGD-35S::p33-BFP, pGD-35S::p33-cYFP, pGD-35S::RFP-SKL, pGD-35S::AtTim21-RFP and pGD-35S::p19 have been described before (Xu et al., 2012, 2014; Xu and Nagy, 2016). To make plasmid pGD-NbPK, the plant *pyruvate kinase* gene fragment was RT-PCR-amplified from the *N. benthamiana* RNA by using oligo-d(T) (for RT) and primers #6660 and #6661 (for PCR). The obtained PCR product was cloned into pGD-35S-L vector at BamHI/SalI sites. To generate plasmids pGD-GFP-PK and pGD-nYFP-PK, the plant *pyruvate kinase* gene fragment was PCR-amplified with primers #6659 and #6660. The obtained PCR product was cloned into pGD-35S::GFP plasmid at BglII/SalI sites or into BamHI/SalI-digested pGD-nYFP-MBP plasmid. To generate plasmids pGD-p33-ATeam$^{YEMK}$ and pGD-p36-ATeam$^{YEMK}$, the TBSV p33 or CIRV p36 sequence was PCR-amplified using primers #1974 / #6793 or #6184 / #6795, respectively. This was followed by the digestion of PCR products with BamHI/XhoI and then, cloned into pGD-35S–L plasmid at BamHI/XhoI sites, resulting plasmids pGD-p33nostop (no stop codon) or pGD-p36nostop (no stop codon at the 3' end of p36 ORF). The ATeam$^{YEMK}$ fragment was PCR-amplified using primers #1293 and #6806, followed by the digestion of PCR product with XhoI/SalI and then, cloned into XhoI/SalI-digested pGD-p33nostop or pGD-p36nostop plasmid, resulting in plasmids pGD-p33-ATeam$^{YEMK}$ and pGD-p36-ATeam$^{YEMK}$, respectively. The *E. coli* expression plasmids pMAL-Ded1, pMAL-33 and pMAL92 were described earlier (Kovalev et al., 2012b; Pogany et al., 2008). The *Agrobacterium tumefaciens* strain C58C1 was transformed with the above pGD-derived plasmids, cultured and used for agroinfiltration of *N. benthamiana* leaves as described (Goodin et al., 2002).

## METHOD DETAILS

### Yeast Transformation and Cultivation

Yeast strains were co-transformed with selected plasmids by using the lithium acetate/ssDNA/polyethylene glycol method, and transformants were selected by complementation of auxotrophic markers (Panavas et al., 2008).

For TBSV replication assays, BY4741, *cdc19*$^{ts}$ and *rpn11-8*$^{ts}$ strains were co-transformed with LpGAD-CUP1::HisFlag-p92 and HpGBK-CUP1::HisFlag-p33/GAL1::DI-72. Transformed yeast strains were pre-grown at 23°C overnight in SC-LH$^{-}$ (synthetic complete media without histidine and leucine) media with 2% galactose. Then, the cultures were transferred to SC-LH$^{-}$ media

supplemented with 2% glucose and 50 μM $CuSO_4$ to launch virus replication at 23°C (permissive temperature), 29°C or 32°C (semi-permissive temperatures) for 24h before sample collection for analysis. In the complementation study, BY4741, *cdc19$^{ts}$* and *rpn11-8$^{ts}$* strains were co-transformed with LpGAD-CUP1::HisFlag-p92, HpGBK-CUP1::HisFlag-p33/GAL1::DI-72 and UpYES (vector control) or UpYES-GAL1::His-CDC19. Transformed yeasts were pre-grown at 23°C overnight in SC-ULH$^-$ media supplemented with 2% galactose. Then, the cultures were transferred to SC-ULH$^-$ media supplemented with 2% glucose and 50 μM $CuSO_4$ to launch virus replication at 23°C or 29°C for 24 h.

To over-express the *N. benthamiana* pyruvate kinase (PK) in yeast, BY4741 was transformed with plasmids UpESC-CUP1::His-p92, HpGBK-CUP1::His-p33/ADH::DI-72 and LpGAD-ADH::PK (or LpGAD as control). The transformed yeasts were pre-grown in SC-ULH$^-$ media supplemented with 2% glucose plus 0.1 mM BCS at 23°C for 24 h and then, the cultures were transferred to SC-ULH$^-$ media supplemented with 2% glucose and 50 μM $CuSO_4$ and grew at 23°C for 24 h. For CIRV replication assays, BY4741 and *cdc19$^{ts}$* were co-transformed with LpESC-CUP1::Flag-p95, HpESC-CUP1::Flag-p36 and UpYC-GAL1::DI-72. Transformed yeasts were pre-grown at 23°C overnight in SC-ULH$^-$ media supplemented with 2% galactose plus 50 μM $CuSO_4$, then the cultures were transferred to SC-ULH$^-$ media supplemented with 2% glucose and 50 μM $CuSO_4$ and grew at 23°C or 29°C for 24 h.

### Virus Strains and Plant Infections

The cDNA clones of TBSV, cherry strain (Hearne et al., 1990) and CIRV, type strain (Burgyan et al., 1996), and cucumber necrosis virus, strain pK2/M5 (Rochon and Johnston, 1991) were used to prepare infectious RNA transcripts *in vitro* with T7 RNA polymerase transcription, followed by inoculation of *N. benthamiana* (lab strain) leaves with ~5 μg RNA transcripts/leaf as described.

### Tombusvirus RNA Analysis

Standard total RNA extraction and Northern blot analysis was performed as described previously (Panavas and Nagy, 2003). To detect either the (+)RNA or (−)RNAs, we prepared the $^{32}$P-labeled DI-72 region III/IV probe with in vitro T7 transcription using PCR-amplified DNA obtained with primers #22 / #1165 for (+)RNA; primers #18 / #1190 for (−)RNAs and HpGBK-His33/Gal1-DI-72 as a template.

### VIGS-based Knockdown of Pyruvate Kinase in *N. benthamiana* Plants

The virus-induced gene silencing (VIGS) in *N. benthamiana* was done as described previously (Dinesh-Kumar et al., 2003; Jaag and Nagy, 2009). The gene accession number of NbPK is Niben101Scf00276g07001.1. We used the cytosolic *N. tabacum* PK sequence (gi|444022|emb|Z29492.1) to do the blast in Sol Genomics database and obtained the predicted cDNA sequence. We analyzed this sequence by the VIGS designing tool provided in Sol Genomics database and identified the silencing target region, which covers the N-terminal part of the PK1 sequence. This region is more variable among the NbPKs (cytosolic and plastid PK).

To generate the VIGS construct (pTRV2-PK), a *pyruvate kinase* gene fragment was PCR-amplified from *N. benthamiana* cDNA using primers #6726 and #6727 and inserted into the corresponding (BamHI and XhoI) restriction sites in plasmid pTRV2. 12 days after the VIGS treatment of *N. benthamiana* (pTRV2-PK together with pTRV1), the level of *N. benthamiana* pyruvate kinase (PK) mRNA was determined by RT-PCR with primers oligo-d(T) (for RT) and #6660 and #6661 (for PCR). We used tubulin mRNA as a control for amplification by RT-PCR using primers #2859 and #2860. Subsequently, the silenced upper leaves of *N. benthamiana* were sap-inoculated with TBSV to launch viral replication. One day later, samples from the inoculated leaves were collected, followed by total RNA extraction and Northern blot analysis as described above. The TRV-cGFP construct (carrying the C-terminal half of the GFP gene not present in *N. benthamiana*) was used as a control.

Protoplasts were isolated from *N. benthamiana* leaves as previously described (Panaviene et al., 2003). Freshly prepared protoplasts were electroporated with 3 μg total RNA obtained from TBSV-infected *N. benthamiana* leaves. Protoplasts were incubated in the dark for 24 h at room temperature and the total RNA was extracted for Northern blot analysis.

### Yeast Cell Free Extract (CFE) Based In Vitro Replication Assay

CFEs from BY4741 and cdc19ts were prepared as described earlier (Pogany and Nagy, 2008; Pogany et al., 2008). Yeasts were grown at 23 °C, reaching 2.0 $OD_{600}$, followed by heat treatment for 1 h at 37 °C. The individual CFE preparations were adjusted to contain comparable amounts of total proteins. The in vitro CFE assay was performed in 20 μl total volume containing 1 μl of adjusted CFE, 0.5 μg DI-72 (+)RNA transcripts, 0.5 μg affinity-purified MBP-p33, 0.5 μg affinity-purified MBP-p92 (both recombinant proteins were obtained from *E. coli*) (Rajendran and Nagy, 2003), 30 mM HEPES-KOH, pH 7.4, 150 mM potassium acetate, 5 mM magnesium acetate, 0.13 M sorbitol, 0.4 μl actinomycin D (5 mg/ml), 2 μl of 150 mM creatine phosphate, 0.2 μl of 10 mg/ml creatine kinase, 0.2 μl of RNase inhibitor, 0.2 μl of 1 M dithiothreitol (DTT), 2 μl of 10 mM ATP, CTP, and GTP and 0.1 mM UTP and 0.1 μl of $^{32}$P-UTP. Reaction mixtures were incubated for 3 h at 25 °C, followed by phenol/chloroform extraction and isopropanol/ammonium acetate (10:1) precipitation. $^{32}$P-UTP-labeled RNA products were analyzed in 5% acrylamide/8 M urea gels (Pogany and Nagy, 2008; Pogany et al., 2008).

In a modified CFE-based in vitro replication assay, which included purified Cdc19, 20 μl of reaction contained 1 μl of adjusted CFE, 0.5 μg DI-72 (+)RNA transcripts, 0.5 μg purified MBP-p33, 0.5 μg purified MBP-p92, 30 mM HEPES-KOH, pH 7.4, 150 mM potassium acetate, 5 mM magnesium acetate, 0.13 M sorbitol, 0.4 μl actinomycin D (5 mg/ml), 2 μl of 150 mM creatine phosphate, 0.2 μl of

10 mg/ml creatine kinase, 0.2 μl of RNase inhibitor, 0.2 μl of 1 M dithiothreitol (DTT), 0.25 mM ATP, 1 mM CTP, 1 mM GTP, 0.01 mM UTP, 1mM ADP, 0.1 μl of $^{32}$P-UTP, 0.34 μM of GST-Cdc19 or GST as a control, and different amounts of PEP substrate (i.e., 0.1, 0.6, 1.2 mM).

### Flag-affinity Purification of Tombusvirus Replicase from Yeast and In Vitro RdRp Assay

BY4741 and *cdc19$^{ts}$* yeasts were transformed with plasmid LpGAD-CUP1::HisFlag-p92 and HpGBK-CUP1::HisFlag-p33/GAL1::DI-72 expressing 6xHis- and Flag-tagged tombusvirus p33 and p92. Yeast transformants were pre-grown in 50 ml of SC-LH$^-$ media supplemented with 2% glucose overnight at 23°C or 29°C, then cultures were transferred to fresh 200 ml of SC-LH$^-$ media supplemented with 2% galactose and 50 μM $CuSO_4$. Yeasts were cultured at 23°C or 29°C until reaching to 2 $OD_{600}$. The tombusvirus replicase was purified as described earlier (Panaviene et al., 2004). Briefly, 2 g of yeast cells were collected by centrifugation and the pellets were resuspended and homogenized in ice-cold high salt TG buffer (15 mM $MgCl_2$, 50 mM Tris–HCl [pH 7.5], 10% glycerol, 0.5 M NaCl, 10 mM KCl, 1% [V/V] yeast protease inhibitor cocktail [Ypic]) by glass beads using FastPrep Homogenizer (MP Biomedicals). The samples were centrifuged at 500× g for 5 min at 4°C to remove glass beads, unbroken cells and debris. The membrane fraction containing the viral replicase complex was collected by centrifugation at 35,000× g for 15 min at 4°C and then solubilized in 12 ml high-salt TG buffer containing 1% Triton X-100, 1% [V/V] Ypic via gentle rotation for 3 h at 4°C. The detergent-solubilized samples were centrifuged at 35,000× g for 15 min at 4°C and the supernatants were incubated with 150 μl anti-FLAG M2-agarose affinity resin (Sigma) pre-equilibrated with 1 ml high salt TG buffer. After 3 h rotation at 4°C, the columns were washed with 15 ml high salt TG buffer containing 0.5% Triton X-100 and 15 ml low-salt TG buffer (15 mM $MgCl_2$, 50 mM Tris–HCl [pH 7.5], 10% glycerol, 0.05 M NaCl, 10 mM KCl,) containing 0.5% Triton X-100. Then, the replicase complex was eluted in 200 μl low salt TG buffer containing 1% YPic and 0.15 mg/ml Flag peptide (Sigma). *In vitro* RdRp activity assay was performed using DI-72 region I/III (−)RNA or region IV (+)RNA as template transcribed *in vitro* by T7 transcription (Li et al., 2010).

### Co-purification of Cdc19p with the Tombusvirus Replication Complex

Yeast strains BY4741, *rpn11-14$^{ts}$* and *rpn11-8$^{ts}$* strains were transformed with plasmids HpGBK-CUP1::Flag-p33 (or HpGBK-CUP1::His-p33 and HpESC-Gal1::Flag-rsGFP as controls), and/or LpGAD-CUP1::Flag-p92 (or LpGAD-CUP1::His-p92 as a control), and UpYES-GAL1::His-CDC19 (expressing a 6xHis-tagged Cdc19 protein). Transformed yeasts were pre-grown in SC-ULH$^-$ media supplemented with 2% glucose for 16 h at 23 °C and then, transferred to SC-ULH$^-$ media supplemented with 2% galactose for 24 h at 23 °C or 32°C. Then, 50 μM $CuSO_4$ was added and the yeast cultures were incubated for 6 h at 23 °C or 32°C. The yeast cultures were then centrifuged, washed with phosphate buffer saline (PBS) and incubated in PBS plus 1% formaldehyde for 1 h on ice to crosslink proteins. Then, glycine (to 0.1M) was added to quench the formaldehyde and the yeast cells were recovered by centrifugation. Yeast cells were broken with glass beads and, after detergent-solubilization (see above), the replicase-complex (containing FLAG-p33 and FLAG-p92 replication proteins) was purified using anti-FLAG M2 agarose (Li et al., 2008). Affinity-purified p33 was analyzed by Western blot using anti-FLAG antibody, and co-purified 6xHis-tagged host proteins were analyzed by Western blot with anti-His antibody.

To analyze the dynamics of host proteins' association with the tombusvirus replicase, the transformed BY4741 (see the paragraph above) were pre-grown in SC-ULH$^-$ media supplemented with 2% glucose for 20 h at 29°C and then, transferred to SC-ULH$^-$ media supplemented with 2% galactose for 24 h at 29°C. The cultures were supplemented with 50 μM CuSO4 for 2.5 h to induce expression of the FLAG-p33 and FLAG-p92 replication proteins. Then, cycloheximide was added (100 μg/ml) to stop protein translation and samples were taken at the 0, 60 and 150-minute time points. Yeast cultures were treated with formaldehyde and processed for FLAG-affinity purification of the detergent-solubilized tombusviral replicase complex, followed by Western blotting as above.

### Recombinant Protein Purification from *E coli*

Recombinant MBP-tagged TBSV p33, its deletion derivatives p33c, pC151-240, pC211-296, pC219-296 and MBP-p92 replication proteins, as well as MBP-Ded1p, and MBP-RH2 were expressed in *E coli* and purified as published before (Kovalev et al., 2012b; Rajendran and Nagy, 2003). Briefly, the expression plasmids were transformed into *E coli* strain BL21 (DE3) CodonPlus. Protein expression was induced by isopropyl-β-D-thiogalactopyranoside (IPTG) at 16°C for 8 h. After collection of the cultures by centrifugation at 4,000g for 5 min, the cells were re-suspended and lysed in reduced-salt column buffer (25 mM NaCl, 30 mM HEPES-KOH pH 7.4, 1 mM EDTA, 10 mM β-mercaptoethanol). The lysate was centrifuged at 14,000 rpm for 10 min to remove cell debris. Then, supernatant was incubated with amylose resin (NEB) at 4°C for 1 h. After washing the resin with 50 ml reduced-salt column buffer (without β–mercaptoethanol), the recombinant proteins were eluted with maltose buffer (column buffer containing 0.18% (W/V) maltose). The affinity-purified proteins were analyzed by SDS-PAGE (Rajendran and Nagy, 2003).

### Recombinant Protein Purification from Yeast

The yeast strain expressing GST-Cdc19 was from the GST-His6 ORF library (Sopko et al., 2006). Briefly, yeast cells were pre-grown in 20 ml SC-UL$^-$ media supplemented with 2% glucose at 29°C for overnight and then, the culture was transferred to 200 ml SC-UL$^-$ media supplemented with 2% galactose and grew at 29°C until reaching 2 $OD_{600}$. Yeast pellets (2 g each) were used to purify the GST-Cdc19p and GST as a control following the procedure described before (Li et al., 2008).

### Cdc19 Pull-down Assay

We have performed this assay as previously described (Barajas et al., 2009b). Briefly, E. coli expressing MBP-tagged p33C or its truncated derivatives were resuspended in ice-cold column buffer (10 mM Tris-HCl [pH 7.4], 1 mM EDTA, 25 mM NaCl, 10 mM β-mercaptoethanol) and lysed by sonication. The cleared lysate was passed through an amylose column to capture the MBP-tagged viral proteins or MBP (negative control). The columns were washed three times with cold column buffer prior to the addition of the yeast lysate. For the pull-down assay, 100 mg of yeast pellets containing His-GST-Cdc19 and its truncated derivatives were resuspended in 150 μl chilled buffer I (20 mM Tris-HCl [pH 7.5], 1 mM EDTA, 200 mM NaCl, 10% [vol/vol] glycerol, 0.1% [vol/vol] NP-40, 10 mM β-mercaptoethanol, 1% [vol/vol] yeast protease inhibitor cocktail [Ypic]) and 1 μl of RNase A (1 mg/ml). Cells were broken in Fast Prep-24 machine by using a 250 μl volume of acid-washed glass beads, followed by the addition of 600 μl of buffer I. After removing the cell debris, the cleared lysates were loaded onto columns with captured MBP-p33C or its truncated variants, followed by incubation at 4°C for 2 h. After washing the columns 5 times with buffer I, the bound proteins were eluted with 50 μl SDS-PAGE sample buffer from the columns and analyzed by Western blotting using an anti-His antibody.

### dsRNA Strand Separation Assay

To analyze the dsRNA strand separation activity present in the *cdc19*$^{ts}$ CFE, first, a TBSV partial RNA/RNA duplex, which contained the full-length unlabeled (+)DI-72 RNA and a $^{32}$P-labeled (−)RI or $^{32}$P-labeled RIII(−) RNAs, were generated as described (Rajendran and Nagy, 2003). Second, dsRNA strand separation assay was performed in 10 μl total volume containing the same amount of BY4741 CFE or cdc19ts CFE together with 5 ng of partial RNA/RNA duplex template and with or without 1mM ATP in a buffer (50 mM Tris-HCl [pH 8.2], 10 mM $MgCl_2$, 1 mM EDTA, 10% glycerol, 200 ng of yeast tRNA [Sigma], and 2 U of RNase inhibitor [Fermentas]) at 25°C for 15 min. After the incubation, the samples were treated with 2 μg of proteinase K at 37°C for 30 min. Then, the samples were analyzed via 5% nondenaturing PAGE performed at 200 V for 1h in a cold room. In addition, this assay was also tested under different conditions, such as providing 0.34 μM of GST-Cdc19p combined with different amount of PEP (0.1, 0.6, 1.2 mM) or using GST-Ded1 (0.5 μM) / MBP-RH2 (0.5 μM) instead of *cdc19*$^{ts}$ CFE.

### Confocal Microscopic Analysis of Yeast Cells

To observe the subcellular localization of Cdc19p in the presence or absence of viral components in yeast cells, BY4741 strain was transformed with plasmids LpGAD-ADH::CFP-p92 (or empty plasmid as a control) and UpYES-GAL1::YFP-CDC19. The transformed yeasts were grown in SC-UL$^-$ media supplemented with 2% galactose at 23°C for overnight. The confocal images were obtained sequentially with an Olympus FV1000 microscope (Olympus America) and merged using Olympus FLUOVIEW 1.5 software (Chuang et al., 2014).

### Co-localization and Bimolecular Fluorescence Complementation Assay in *planta*

To analyze the localization of pyruvate kinase in plants, *N. benthamiana* leaves were ago-infiltrated with plasmids pGD-35S::p33-BFP ($OD_{600}$ ~0.3), pGD-GFP-PK($OD_{600}$ ~0.3) and pGD-35S::p19 ($OD_{600}$ ~0.3) or the plasmids : pGD-35S::p33-cYFP (OD~0.25), pGD-35S::p92-CYFP ($OD_{600}$ ~0.25), pGD-nYFP-PK or pGD-nYFP-MBP ($OD_{600}$ ~0.25), pGD-35S::RFP-SKL($OD_{600}$ ~0.25) and pGD-35S::p19($OD_{600}$ ~0.25) for BiFC assay (Xu and Nagy, 2016). At the 48 h time-point after agro-infiltration, live confocal images were obtained with an Olympus FV1000 microscope (Olympus America). BFP/Alexa 405, GFP/Alexa 488, and RFP were excited using 405 nm, 488 nm, or 543 nm lasers, respectively. Images were obtained sequentially and merged using Olympus FLUOVIEW 1.5 software (Xu and Nagy, 2016).

### Visualization and Measurement of ATP Levels in Yeast

Intracellular ATP levels were visualized using the ATeam-based biosensor (Imamura et al., 2009) by using a confocal microscope and measured by FRET analysis. To analyze the ATP level in the TBSV replication compartment in yeast, BY4741, cdc19ts, rpn11-8ts or rpn11-14ts were transformed with plasmids LpGAD-ADH::ATeam$^{YEMK}$–p92 (or LpGAD-ADH:: ATeam$^{RK}$–p92 as a control), UpYC-GAL1::DI-72 and HpESC-GAL1::p33/GAL10::pex13-RFP. The transformed yeast cells were pre-grown in SC-ULH$^-$ media supplemented with 2% glucose at 23°C for overnight and then, transferred to the fresh SC-ULH$^-$ media supplemented with 2% glucose for 4h at 23°C or 29°C. To observe the dynamics of ATP levels within the TBSV replication compartment during virus replication, the transformed yeast cells were pre-grown in SC-ULH$^-$ media supplemented with 2% glucose at 23°C for overnight and then, transferred to the fresh SC-ULH$^-$ media supplemented with 2% galactose at 23°C. Samples were harvested at 4, 8 and 12 h time points for the confocal microscopy analysis.

In the case of CIRV, yeast BY4741 and *cdc19*$^{ts}$ were transformed with plasmids HpESC-CUP1::ATeam$^{YEMK}$-p95 (or HpESC-CUP1::ATeam$^{RK}$-p95 as a control), HpESC-CUP1::p36 and UpYC-GAL1::DI-72. The transformed yeasts were grown in SC-ULH$^-$ media supplemented with 2% glucose plus 50 μM $CuSO_4$ at 29°C for overnight, followed by confocal microscopy analysis as described above.

To detect the cytosolic ATP levels during on-going TBSV replication, yeast BY4741 strain was transformed with plasmid LpGAD-CUP1::HisFlag-p92, UpYES-GAL1::ATeam$^{YEMK}$ and HpGBK-CUP1::HisFlag-p33/GAL1::DI-72 or HpGBK-CUP1::His-p33 (or empty plasmid as a control). The transformed yeasts were pre-grown in SC-ULH$^-$ media supplemented with 2% glucose at 23°C for

overnight and then, transferred to SC-ULH$^-$ media supplemented with 2% galactose plus 50 μM $CuSO_4$ at 23°C for overnight. Then the cultures were refreshed in SC-ULH$^-$ media supplemented with 2% glucose at 23°C for 1 h, followed by confocal microscopy analysis as described above.

Confocal FRET images were obtained with an Olympus FV1000 microscope (Olympus America). Cells were excited by a 405-nm laser diode, and CFP and Venus were detected at 480–500 nm and 515–615 nm wavelength ranges, respectively. Each YFP/CFP ratio was calculated by dividing pixel-by-pixel a Venus image with a CFP image using Olympus FLUOVIEW software or ImageJ software.

### Visualization and Measurement of ATP Levels in Plants

To detect the ATP levels within the tombusvirus replication compartment in plant cells, in the case of TBSV, the pyruvate kinase (PK) silenced N. *benthamiana* plants (see above) or control plants were co-agroinfiltrated with plasmids pGD-p33-ATeamYEMK, pGD-DI-72, pGD-35S::RFP-SKL, pGD-35S::p19 and/or pGD-p92. In the case of CIRV, the PK-silenced or nonsilenced *N. benthamiana* leaves were co-agroinfiltrated with pGD-p36-ATeamYEMK, pGD-35S::p95, pGD-35S::AtTim21-RFP, pGD-35S::p19 and/or pGD-DI-72. The images were taken at 2.5 and 3.5 days post-agroinfiltration and analyzed with the method described above.

## QUANTIFICATION AND STATISTICAL ANALYSIS

All the Northern and Western blot signals were detected using a Typhoon 9400 image scanner (Amersham) and quantified by ImageQuant software. In virus replication assays, all the samples were normalized based on the 18S ribosomal RNA level. Results from three different experiments including 9-12 separate biological samples were used to calculate the standard deviation and shown as plus/minus value.